FIELD EMISSION FROM AMORPHOUS CARBON THIN FILM HAVING EMBEDDED NANOPARTICLES

A Dissertation submitted in partial fulfillment of the requirements for the degree of

Master of Technology

(Nanoscience and Technology)

Prabhakar Singh

2k09/NST/09

Delhi Technological University

Formerly Delhi College of Engineering

Main Bawana Road,Shahbad Delhi-110042

FIELD EMISSION FROM AMORPHOUS CARBON THIN FILM HAVING EMBEDDED NANOPARTICLES

A Dissertation submitted in partial fulfillment of the requirements for the degree of

Master of Technology

(Nanoscience and Technology)

By

Prabhakar Singh

2k09/NST/09

Under the Supervision of

Dr. O.S. PANWAR

Scientist G & Head (Deputy Director),

(Plasma Processing of Materials, Devices and Systems)

National Physical Laboratory (CSIR)

Submitted to

Delhi Technological University

(Formerly Delhi College of Engineering)

Main Bawana Road,Shahbad Delhi-110042

CERTIFICATE

This is to certify that dissertation titled **"FIELD EMISSION FROM AMORPHOUS CARBON THIN FILM HAVING EMBEDDED NANOPARTICLES"** is submitted by **Prabhakar Singh** (2K09/NST/09) towards the partial fulfillment of M.Tech Degree in Nanoscience and Technology under the supervision of **Dr. O.S Panwar**. This Work was performed at **National Physical Laboratory,** Delhi from 2 July 2010 to 30 june 2011. The work has not been submitted elsewhere for the award of any degree.

Dr. O.S.Panwar
Scientist G & Head (Deputy Director),
(Plasma Processing of Materials, Devices and Systems)

Dr. Rajiv Chopra
Head HRD
National Physical Laboratory

Date_____

Place_____

_____

(Examiner)

ACKNOWLEDGEMENT

I would like to take the opportunity to acknowledge my indebtedness towards all the people who have helped me in all my tasks and works.

My sincere gratitude is directed to my supervisor; Dr O.S Panwar. He actively involved himself in the project and offered useful support at every stage of my project, reviewed my schematics, answered my all questions and provided me with books and reading material.

With profound appreciation and sincere indebtedness, I express my deep gratitude to Dr. R.K Sinha, HOD, Department of Physics, DTU for granting me the permission to do project work at NPL. His constant encouragement and interest was instrumental in the completion of project. I am also thankful to all of my faculty members of the department for their valuable suggestions time to time.

I would like to thank our Course coordinator Dr. P.K.Tyagi for his constant support and encouragement.

I would like to acknowledge my friends and teachers at *Delhi Technological University, Delhi* who were kind enough to help me during my course work and teaching me with the best of their knowledge.

To the class of 20009-11, thank you for the very interesting and enjoyable two years!

I owe my loving thanks to my Parents, my brother, my sister and friends. They have supported me very much during my study and research. Without their encouragement and understanding it would have been impossible for me to finish this work.

I am thankful to all members of amorphous and microcrystalline Silicon Solar Cell Group, in general, and Mr. Ravi Kant Tripathi in particular who helped in this work.

Prabhakar Singh

TABLE OF CONTENTS

CHAPTER 1

INTRODUCTION

At the present time, there are many aspects in our personal life that are going to be transformed by nanotechnology. Not only are computers and electronic devices getting smaller, more powerful and cheaper, but nanotechnology has also become more advanced as we can manipulate matter at the molecular and atomic level. Nanostructured materials and devices provide links between molecular and solid-state physics and eliminate some of the limitations of conventional technologies. These nanostructures have the potential for applications such as battery electrodes, gas sensing, supercapacitors and field emission display for flat-panel TVs. Hence researchers are focused on investigating and developing nanostructured materials, particularly silicon nanostructures that can be combined with the power of modern silicon integrated circuits.

Emerging vacuum microelectronics devices are of much interest due to their unique properties such as high current densities, ballistic electron transport, temperature independence and radiation hardness. These properties promote a wide range of applications including field emission displays (FEDs) for flat panel monitors. Many research groups have developed field emission devices based on nanostructured material such as carbon nanotubes (CNTs), nanobelts, SiC nanowires, AlN nanoneedles, Si nanowires, SnO nanowhiskers and so forth. Generally, fairly high emission current density, i.e. 10mA/cm^2, is desirable to light a phosphor display.

This chapter provides the outline of this thesis. It lays out the background of amorphous diamond like carbon, vacuum electronics and potential applications that has motivated this research.

1.1 Motivation

Many nanostructured materials have been used to fabricate field emission devices; a motivation to investigate the capability of amorphous diamond like carbon as field emitters in vacuum microelectronic devices is enormous due to its promising property. The challenge now is to produce the amorphous diamond like carbon using various types of techniques and investigate their formation mechanisms, electrical characteristics, lifetime, stability and potential applications. This research also aims to optimise the growth conditions of amorphous diamond like carbon and test the properties of field emission in order to produce a vacuum microelectronics device that is uncomplicated and inexpensive to produce.

1.2 Overview of Vacuum Electronics

The practice of using controlled electron propagation in a vacuum to obtain signal gain has been around since American inventor Lee De Forest introduced the triode vacuum tube in 1907 [1]. Vacuum electronics use the mechanism of electron emission into a vacuum. By fabricating arrays of conductive or semiconductive structures that are either gated or ungated, the devices can be formed by utilizing cold emission and ballistic transport of electrons from emitting cathodes to appropriate collector electrodes. Integrated solid-state devices have taken over as cheap, versatile and robust alternatives to vacuum electronics. However, there are certain applications where solid-state devices are impractical, and a potential solution is the same vacuum technology that has been forgotten for nearly 50 years. Potential applications include flat panel vacuum displays[2] , ultrahigh-frequency power sources and amplifiers, e.g. microwave tube power amplifiers, electron and ion guns and x-ray sources, high- speed logic and signal processing circuits, miniature electron-beam lithography systems, electron microscopes and microprobes, and sensors[3] .

Vacuum electronics can be separated into two categories: thermionic emission or field emission. The difference between these two categories is the way electrons are emitted from the cathode. In both cases, the emitted electrons are accelerated towards the anode through a vacuum channel.

1.2.1 Thermionic Emission

Thermionic emission relies on a cathode which is a heated electron emitter. The cathode is heated up until the electrons receive enough kinetic energy to leave the surface of the cathode. Thermionic devices have the obvious disadvantage that every device needs a heating element. Thus, the material used in these devices must be able to tolerate a temperature of at least 1000K to induce electron emission.

1.2.2 Field Emission

Unlike thermionic emission, field emission is possible with a cold cathode. Although field emission has the obvious advantage of not requiring a heating element, the fabrication of these devices presents multiple problems. The field emission highly depends on the size and work function of the emitter. A cold cathode becomes more power efficient as smaller emitter sizes are achievable using modern IC fabrication processes. Therefore, field emission is the preferred integrated solution. Field emission occurs when an electric field above approximately 0.5V/Å is placed on a metal surface in a vacuum [4]. The electric field at the emission site is normally enhanced over the averaged electric field by a factor according to the geometrical structure of the emission site. This factor is almost inversely proportional to the curvature radius of the tip of the emission site [5]. Therefore, researchers have emphasized the need for reliable and reproducible fabrication of sharp emitter structures. One of the promising field emitters with low work function and high field enhancement factor is Diamond like carbon thin having novel nano structures. Many research groups have developed innovative nanostructure fabrication techniques to improve the aspect ratio and hence the field emission.

A negatively charged cathode is used in a field emission device. This type of display uses an applied voltage to create an enhanced electric field at emission sites those electrons can engage in a phenomenon known as tunneling as escape into free space without need for heating the cathode to release electrons. Normally, in order to escape the conductor, electrons must have enough thermal energy to overcome that potential energy barrier. By supplying an external electric field, the conductor changes the shape of the potential energy barrier charges, becoming thinner and thinner as the electric field increases. Eventually, the electrons can go all the way through the barrier.

In general, the current-voltage characteristics of field-emission between the cathode tip and anode was confirmed, expressed by the Fowler-Nordheim equation [6];

$$I = A(\beta E)^2 \exp(-B\phi^{3/2}/\beta E) \quad \text{..... (1.1)}$$

Where I is the current in amperes, Φ is the barrier height in eV (1.6×10^{-19} J), E is the electric field in V/m, β is the field enhancement factor at sharp geometries, and B = 3.06×10^9 for carbon and A = 1.4×10^2.

Vacuum field emission devices have become a promising candidate for emerging display technology due to their interesting properties compared to conventional thermionic emission devices that require high temperature and power to operate. Unlike thermionic emission, field emission devices can induce the electrons to emit at low temperature; sharp and thin emitters on the cathode are desired in order to increase the field emission. Many candidates from other research groups, such as carbon nanotubes (CNTs), SiC and ZnO, appear to have high field emission, but their complicated fabrication processes are the drawback.

1.3 Potential Applications

The amorphous carbon thin film structures can be applied in many applications, including optoelectronics, sensors, x-ray sources and cathodes in vacuum microelectronics. Most of those applications utilize their high aspect ratios that provide high field emission with low voltage operation power consumption. Similar to conventional thermionic vacuum microelectronic devices, field emission devices can be used as active elements in circuits, particularly in integrated circuits; due to their small sizes. The ballistic electron transport in vacuum microelectronics devices provides short transit times compared to solid state devices. Thus field emission devices are able to operate at higher frequencies with adequate efficiencies. However, at low frequencies, field emission devices create fluctuation noise for high current which may not be suitable in some applications.

The typical application described here is a field emission display (FED), which has been a prospective flat screen technology for over 20 years but reliability and longevity issues have

prevented it from leaving the laboratory. Unlike the thermionic cathode in conventional Cathode Ray Tube (CRT), the field emission cathode can operate at low temperatures, hence no warming up time and high power are required. FEDs not only conserve the image quality and viewing angles of CRT, but they also provide high brightness, reduced display depth, and lower power consumption, making them suitable for larger flat screens. Samsung demonstrated a working CNT display prototype of field-emission display with 30 inch diagonal screen in 1999 [7].Amorphous diamond like carbon have similar properties as CNTs; they certainly are alternative field emitters which can be easily produced in a very short time.

CHAPTER 2

EXPERIMENTAL TECHNIQUES AND PROCESS

Generation of Vacuum

2.1 - What is Vacuum

The atmospheric air around us is said to contain nearly 2.5 x 10^{19} molecules for every cubic centimeter space. Any given space having molecular density less than this is said to be under "vacuum" conditions. A vessel with necessary pumping and vacuum measuring equipment are referred to as a vacuum system and the technology dealing with the production of such reduced-pressure environments using different scientific concepts is known as "vacuum technology".

Vacuum technology is fundamental to a range of scientific explorations and technological processes; extending from analyzing atomically clean surfaces at extremely low pressures of the order of 10^{-11} Torr (1Torr = 1mm Hg ,1 milli bar[mbar] = 0.75 Torr = 10^{-2} Pascal[pa]) to freeze-drying of foodstuffs at relatively high pressures in the range of 10^{-1} Torr. Vacuum conditions between these extremes are required for TV tube production, vacuum furnaces, vacuum coating, semi-conductor processing, particle accelerators, space simulation, etc.

It is interesting to know that we, human beings, continuously create vacuum during respiration and suction. Another natural phenomenon is the decrease in atmospheric pressure with an increase in altitude (by a factor of 10 for every 15 km), from 760 Torr at sea level to a pressure of 10^{-3} Torr at an altitude of 90 km. Above 100 km, atmospheric pressure decreases relatively slowly (by a factor of 10 for every 100 to 200 km) resulting in ultra-high vacuum (UHV) of the order of 10^{-19} Torr at 1000 km. It is to be noted here that such clean UHV conditions (< 10^{-10} Torr) obtained in a limited space on earth by complicated expensive technologies are naturally available in an infinite large volume of deep space beyond 1000 km altitude. This natural facility is presently being explored for useful exploitation by mankind. The vacuum systems can be classified according to the pressure range in which they operate: Rough, High, Very high and Ultra high vacuum. The type, size and no. of components used vary with these classifications.

2.2 – Classification of vacuum pumps

Because of natural inherent limitations, no single vacuum pump exists which can cover the pressure range from 760 to 10^{-10} Torr. Hence, depending on the ultimate pressure needed in the vacuum system, combinations of different types of vacuum pumps have to be used for different applications. There are two basic approaches to reduce the pressure in a vacuum vessel as

(1) The removal of the gas molecules from the vessel and exhausting them from the system.

(2) The removal of the gas molecules from the gas phase and retained them into the system.

On the basis of these approaches the vacuum pumps are broadly classified into two groups.

(1) Those which follow the first approach such as

Mechanical pumps: Rotary pumps, Root blower pumps, Turbo molecular pumps.

Vapor pumps: Diffusion vapor pumps, Ejector pumps.

(2) Those which follow the second approach such as Ion getter pumps, Adsorption pumps etc.

In this present study we used rotary pump and turbo molecular pumps. A brief description of these two pumps is written in the following.

2.2.1 – Rotary vane pump

The rotating vane pump, known also as Rotary pump, is a simple and most popular positive displacement pump. Figure 2.1 shows the cross-section and exploded view of a typical rotating vane pump. It has a cylindrical steel rotor located eccentrically in cylinder stator housing, almost touching the stator surface at the top. The rotor is slotted at its diameter to take two spring-loaded vanes which bear tightly against the inner surfaces of the stator.

The stator is a steel cylinder the ends of which are closed by suitable plates, which holds the shaft of the rotor. The stator is pierced by the inlet and exhaust ports which are positioned respectively a few degrees on either side of the vertical. The inlet port with a dust filter is connected to the vacuum system and the exhaust port is provided with a valve, which may be a

metal plate moving vertically between arrester plates, or a sheet of Neoprene, which is constrained to hinge between the stator anda meatels.

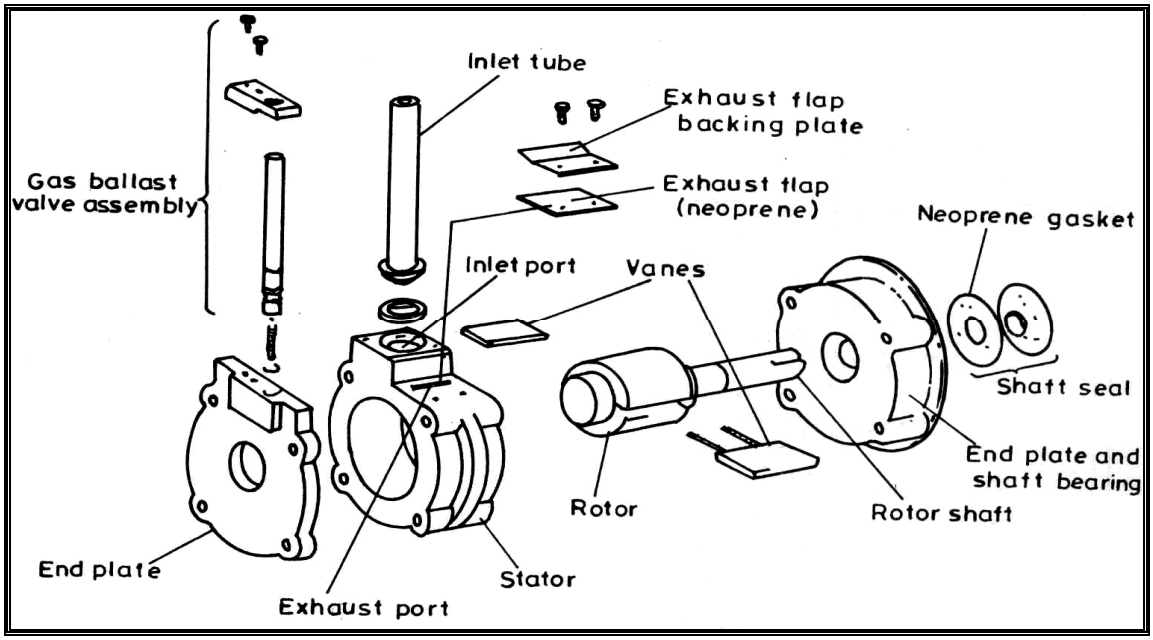

Fig: 2.1 Exploded view of a rotating vane pump.

The line of contact known as the top seal between rotor and stator must have a clearance of 2-3 microns. All of the contacting surfaces are ground to a high precision and the whole stator–rotor assembly is submerged in suitable oil, which serves as a sealant, coolant and lubricant. A film of oil is used on all moving parts. The rotary oil-sealed pumps normally operate at speeds of several hundred revolutions per minute. They are air cooled in the smaller sizes and water cooled in the larger sizes. Pumps with capacities ranging from a few tenths to over a thousand cubic feet per minute are available commercially.

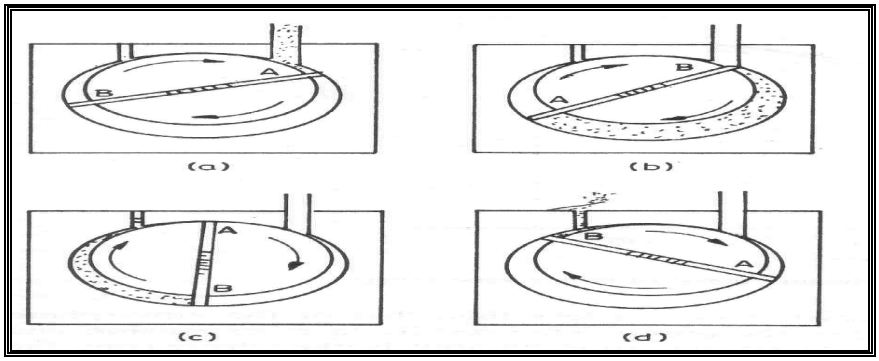

Fig. 2.2: Action of the rotating-vane pump.

The action of the pump is shown in Figure 2.2. As vane A passes the inlet port, the vacuum system is connected to the space limited by the stator, the top seal, the rotor and vane A. The volume of this space increases as the vane sweeps round, thus producing a pressure decrease in the system. This continues until vane B passes the inlet port, when the volume of the gas evacuated is isolated between the two vanes. Further rotation sweeps the isolated gas around the stator until vane a passes the top seal. The gas is now held between vane B and the top seal, and by further rotation it is compressed until the pressure is sufficient (about 850 Torr) to open the exhaust valve, and the gas bubbles out through the oil to the atmosphere. As the contacts of vanes and rotor with stator are required to make vacuum tight seals, the inner surface of the stator and outer surfaces of the rotor and vanes, are very carefully machined. It is also necessary to ensure that no abrasive material or gas which is likely to corrode the metal surface enter the pump chamber. The minimum space between the rotor and stator where it approximately touches may be few microns. Since both vanes operates in one rotation of the rotor, a volume of gas equal to twice that indicated in Fig.2.2b is displaced by the pump. Thus, the volume rate at which gas is swept round the pump, referred to as pumping speed 'S' (liters/sec)is given by,

$$S = 2 \times (V \times n) \qquad \ldots\ldots. (2.1)$$

Where V is the volume of vanes A and B in liters and n is the number of rotations per unit time. The pumping speed is quoted at pressure prevailing at the inlet and hence is expected to be constant regardless of the pressure as V is constant. But in practice, the pumping speed is fairly constant at high pressures (760 – 10 Torr), falls appreciably at lower pressures, and becomes zero at ultimate pressure (Fig. 2.3). This can be understood in the following manner.

In a rotary pump, the gas is compressed into a small but finite dead volume before getting discharged. When the system pressure becomes so low, at maximum compression, the gas pressure is still less than that of the atmosphere and it cannot be discharged from the pump. This results in re-expansion and recompression of the same gas inside the pump without further decreasing the pressure in the system. The ratio of the exhaust pressure to the inlet pressure is termed as the pump compression ratio. Thus, to produce pressures even of the order of 10^{-2} Torr, a compression ratio of the order of 10^{5} is required. To produce a vacuum better than this, a two-stage pump where the exhaust of first stage is connected to intake of second stage is used. Here the overall compression ratio is much higher (product of individual ratios) to exhaust the gas

from the system at much lower pressures (10^{-3} Torr). Parallel connection of two identical rotor systems will provide twice the displacement but the same ultimate pressure as there is no change in the compression ratio.

In addition to the above criteria, the pumping at lower pressures is also limited by unavoidable leaks across top seal and other sealing surfaces, and by the finite vapor pressure of the lubricating oil. The pump oil is usually hydrocarbon oil chosen for its low vapor pressure. The oil must also possess appropriate viscosity for the pump, since too low a viscosity will result in noisy pump operation and too high a viscosity may result in seal failure, loss of vacuum and possibly pump seizure. Freeze up of the pump may occur if improper oil is used which does not provide adequate lubrication and allows the pump to overheat and expand. In addition freeze up can also occur from chemical cracking of the oil or from foreign materials entering the pump.

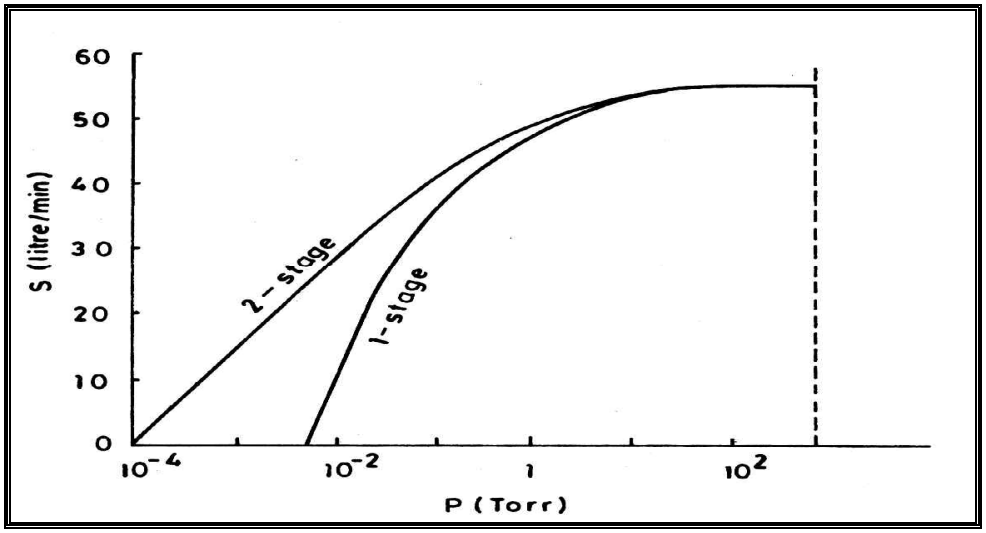

Fig. 2.3: Typical pumping-speed pressure curve of rotary vane pump.

The pump should be vented back to atmosphere as soon as it is stopped as otherwise the oil in the pump will enter into the system due to suction. During unattended operation, this situation may occur due to power failure. Solenoid valves can be used to close off the pump from the rest of the system and to vent it to atmospheric pressure if the power is turned off. Further, a reservoir to catch the oil is added b/w the pump and the system as a safety precaution. Further, inlet filters are added to filter glass particles or abrasive materials that may be present in the system under evacuation.

The most severe problem normally faced while using mechanical pumps is that of contamination of the system by the pump. The contamination from the pump mainly arises due to hydrocarbon pump fluids, where their vapor pressure and that of their cracking products at room temperature is in the range of several milli-torr. The pump fluids will migrate from the pump back to and throughout the vacuum system, particularly at low pressures when pumping line is in the molecular flow region. This hydrocarbon combination can be minimized with liquid nitrogen or absorbing traps.

Most vacuum pumps are available with a feature called gas ballast, or vented exhaust. This is a device to minimize condensation of vapors in the pump. The gas ballast feature helps to minimize the compression ratio to which the condensable vapor is subjected. Atmospheric air is subjected to the pump body during the compression stroke. Since the exhaust valve opens when the pressure inside the pump is just above atmospheric, the mixing of no condensable air with the condensable vapor reduces the ratio of compression for the partial pressure due to the condensable vapor. As might be expected, this causes some deterioration of the ultimate pressure of the pump, especially in a single stage pump. For this reason the gas-ballast valve is usually adjustable, so that, once the gas-ballast is no longer needed, the good ultimate pressure of the pump can be regained by closing the ballast.

2.2.2 – Turbomolecular pump

Turbo-Molecular (turbo) pumps Fig 2.4 are very clean mechanical compression pumps. They pump by using a high speed rotating surface to give momentum and direction to gas particles. They operate smoothly and contribute little low frequency vibration to the operating system. They are the only purely mechanical vacuum pump that can reach pressures of less than 5×10^{-10} Torr without using traps. (Metal gaskets and a mild bake out are necessary to reach this pressure.)

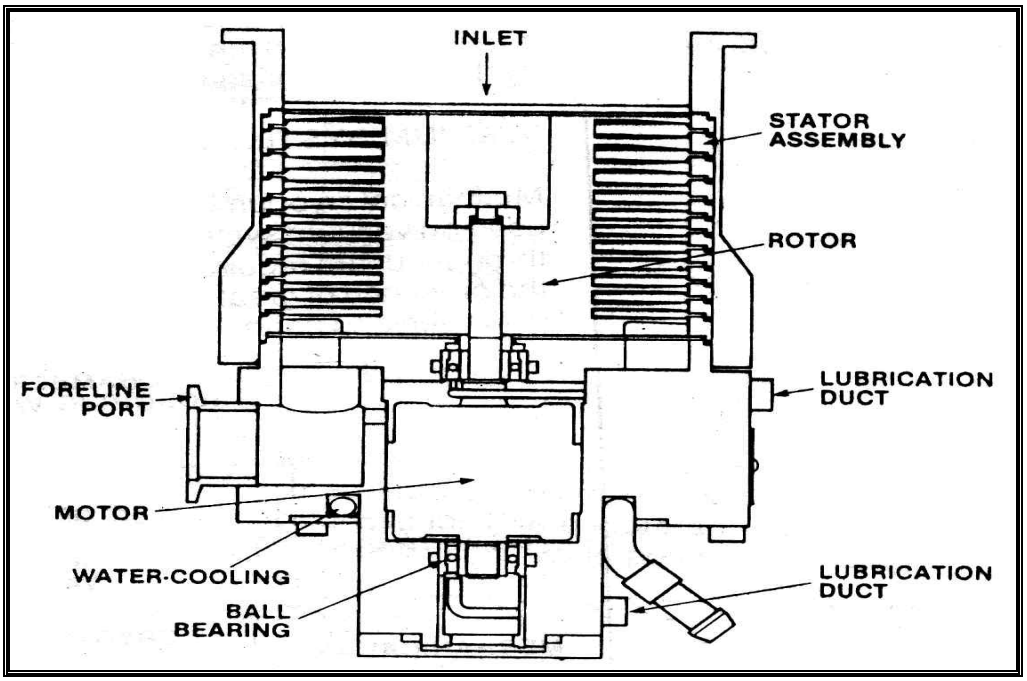

Fig.2.4 Turbomolecular Pump

Under most circumstances, turbo pumps are highly dependable and clean. Because they can operate from pressures as high as 20 milli Torr to below 5 x 10^{-10} Torr, turbo are used in a wide variety of applications. They are ideal for uses where a vacuum relatively free of hydrocarbons is a must. Turbo pumps offer the advantages of clean operation and quick start-up. The turbo pump cannot exhaust directly to atmosphere. Though usually backed by a rotary mechanical pump, turbo are occasionally also backed by other types of pumps.

The turbo pump is mainly composed of rotating and fixed disks. These are called rotors and stators, respectively. The rotor disks are arranged alternately with the stator disks. On each disk are blades. A disk may have from 20 to 60 blades. The pitch and number of blades on a disk determines its ability to compress gases at a given speed.

Each rotor-stator combination can be called a pumping stage. Several rotor-stator pumping stages that have the same blade pitch make up a compression stage. A pump may have as many as twenty stages. The rotor is driven by a motor capable of reaching speeds from 20,000 to 60,000 rpm. The motor is typically powered through a special power supply. Compressed gases are expelled from the pump via a foreline which must be evacuated by some type of backing pump.

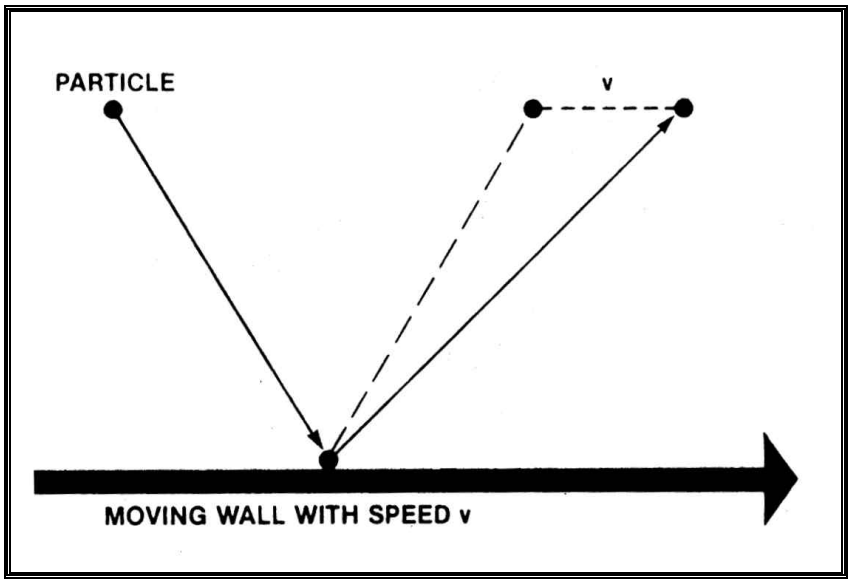

Fig. 2.5 Gas molecule striking a surface

When a gas molecule strikes a surface Fig 2.5, it keeps its own speed it also picks up a little more speed and a slightly different direction when in contact with the moving surface. By this process, the movement of molecules can be directed, and pumping takes place. The turbo pump works much like this; however, it adds blades to the moving surface plus a closed-coupled stator. The stator also has blades. Each blade, when moving, will give some momentum to the gas molecules it hits. Each rotor blade, than, acts as a molecular pump. Which yields is much greater momentum, speed and direction are given to gas molecules entering this pump. In the molecular flow range, the gas particles collide much more often with the moving vanes than with each other. The effect of moving vanes on the gas particles is highest in the molecular flow range. Pump operating on this principle are called molecular pumps.

On the stages closest to the inlet, the blades have a large angle so as to pump at a faster rate, because more “open” space accesses the chamber. The blades closest to the foreline have a small angle for greatest compression. This works to move the gases from the inlet into the foreline. It also works to keep the gas and oil molecules in the foreline from making their way to the inlet.

Turbo pumps typically operate at speeds ranging from 20,000 to 60,000 rpm. When the turbine speed drops to less than 60% of its nominal speed, gas or oil molecules can make their way from the foreline, past the inlet, and into the chamber. This can contaminate the pump and the product

or process. Typical causes can be an overpressure condition in either the chamber inlet or pump foreline.

The worst situation for a turbo pump is a hardware ‘crash’. This is usually caused by debris falling into the pump inlet and touching the rotor blades. A ‘crash’ literally destroys the internal pump stages. The pump must usually be replaced after this experience.

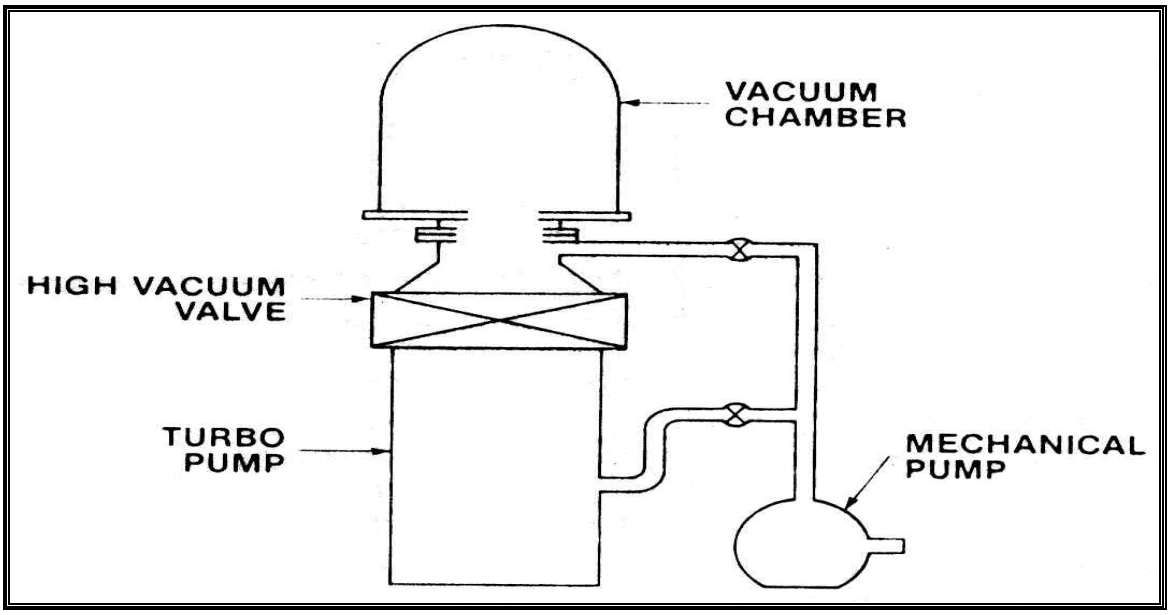

Fig 2.6 Design of pumps system

Most system designs use the turbo pump coupled with a high vacuum valve. This design is similar to a diffusion-pumped system using a common roughing and fore line pump as shown in Fig 2.6. It is possible, however, to rough pump a chamber right through the turbo; in this case, as chamber pressure is reduced, the turbo will gain speed. This type of system design should not be used if the work chamber needs to be vented to high pressure with any frequency, or if rapid pump down to low pressure is required. Turbo pump can be also placed in series with cryotraps to promote high speed pumping of water vapor and other condensable.

Contamination with forepump oil or bearing oil may prevent pumping below 10^{-5} Torr. The pump and system should be cleared with the appropriate solvents. Typical turbo pump maintenance includes changing the lubricating oil, when present, at recommended intervals. Bearing wear is expected. Due to the precision balance and tolerances involved, bearings are normally replaced by factory trained personnel. Turbo must generally be rebuilt yearly.

2.3-Pressure measurement in vacuum systems

The pressure in vacuum systems is defined as the force exerted by the gas per unit surface area. Pressure measurements can be made by using direct (absolute) or indirect techniques. In the direct (absolute) method, the pressure is measured directly as force exert on a solid surface or liquid column. The calibrations of these gauges are done by their geometry and these gauge measure the pressure accurately for all the gases. But in indirect gauges for the measurement of the pressure, pressure related characteristics of the gases are measured. Since these characteristics depend upon the type of the gas, thus these gauges are calibrated with absolute gauge before being used for different gases. The most important problem with pressure measurement is the choice of the proper gauge in a given situation. Thus, for the correct choice of the gauge the knowledge of the working principle of the gauge, range of the pressure in which it can used and its accuracy in that range is necessary.

2.3.1 Classification of gauges

Gauges are classified in the following two broad categories

(1). Total pressure gauges and (2). Partial pressure gauges.

(1). Total Pressure Gauges : The working of these gauges is based on different physical principles, the following gauges are designed.

Mechanical gauges (absolute or direct gauges) : Bourdon, Diaphragm, Liquid manometers and McLeod.

Thermal conductivity gauges (indirect gauges): Thermocouple and Pirani.

Ionization gauges (indirect gauges): These gauges are of two types:-

Hot-cathode gauges: Schulz and Phelps, Conventional, Bayard- Alpert, Orbitron, and Magnetron.

Cold-cathode gauges: Penning, Magnetron, Inverted Magnetron.

(2). Partial Pressure Gauges: Mass-spectrometer, Quadrupole and Monopole mass spectrometers.

In the present study, we used the Pirani and Penning gauges. Let us discuss about them in brief.

2.3.2 Pirani gauge

The Pirani gauge utilized the change in electrical resistance of the wire with temperature. The filament's resistance is measured with the Wheatstone bridge network which also supplies the power to heat the filament. A simple form of the circuit is shown in Fig 2.7.

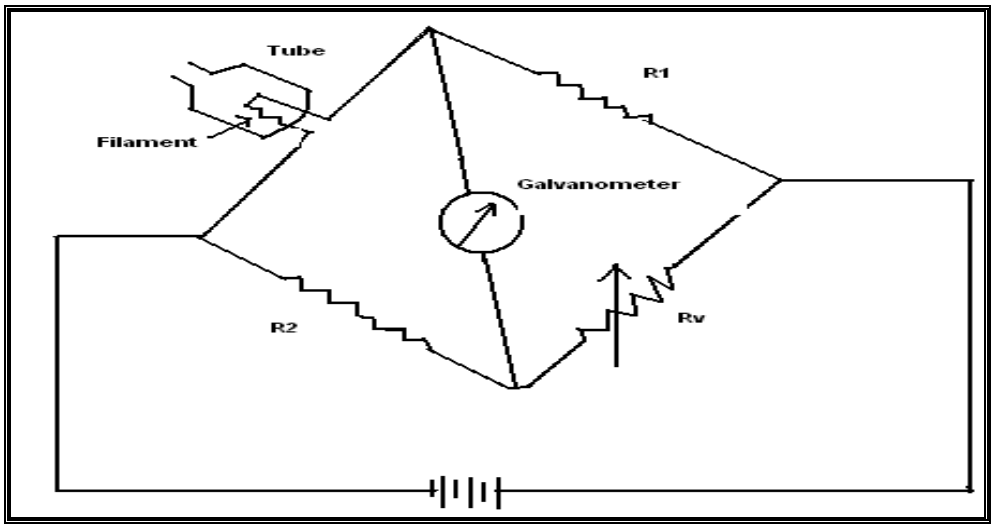

Fig. 2.7 Pirani Gauge

The wire filament of the gauge (Rg) forms one arm of the bridge. The two arms (R1 and R2) have fixed resistance close to that of the filament. The resistance of the fourth arm (Rv) is variable, which allows the bridge to be balanced. The bridge is balanced when the galvanometer reads zero current. Balancing of the bridge is done with the gauge tube at a very low pressure (pressure lower than the gauge limits). Any increase in the pressure causes a wire temperature and increase its resistance. This change unbalanced the bridge and causes a current flowing through the galvanometer and gives the pressure measurement. The operating range of the most of the pirani gauges are from 2Torr to $4* 10^{-4}$Torr.

2.3.3 Penning gauge

This gauge also called cold cathode ionization gauge. This gauge is based on the glow discharge which occurs in the gas at low pressure in the presence of a magnetic field. The geometry of the gauge is quite simple. It consists of two cathode plates parallel to each other with a ring shaped anode in a space between them. It can be shown in Fig 2.8.

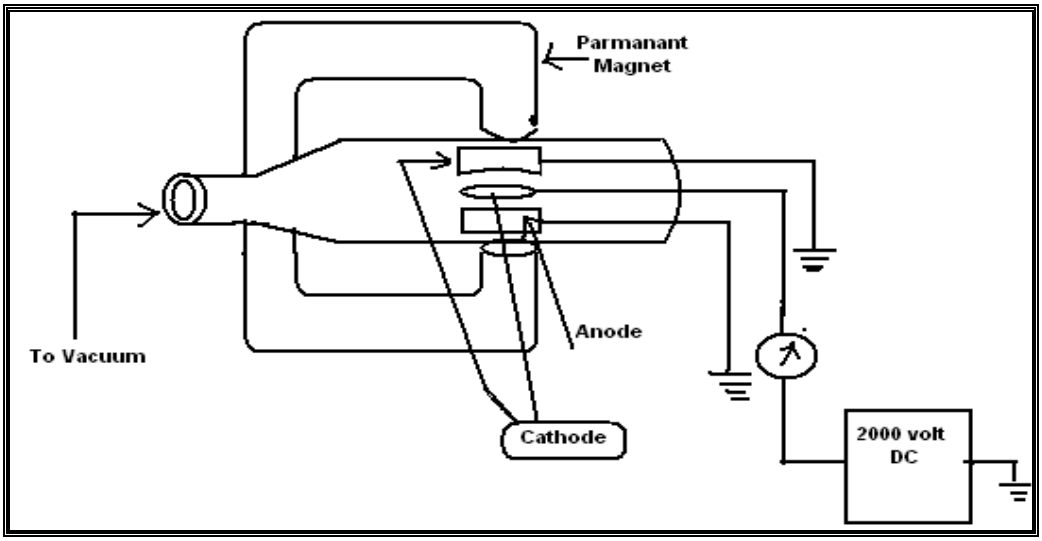

Fig. 2.8 Penning gauge

A direct current voltage of 2000 V (approximate) is supplied between cathodes and anode and a magnetic field approx. 400 G is normal applied to the cathode surface. Electrons which originated in one or other cathodes do not go directly to the anode because the magnetic field gives a spiral path to the electrons. This increases the path length of the electron due to which no. of collisions increases as a result the ionization probability also increases even at lower pressure. The positive ions are attracted by the cathodes. The total discharge current which is the sum of the positive ion current to the cathodes and the electron current from the cathode is used to measure the pressure. This gauge is used from the upper limit of the pirani gauge and measure the pressure up to 10^{-6} Torr.

2.4 Various forms of Carbon

2.4.1 Carbon

Carbon is an abundant chemical element in nature. It constitutes one of the basic elements for life and is widely used in industry for materials manufacturing. The fundamental feature of carbon is its unique capability for combining with other elements. The so called hydrocarbons are formed by the grouping of carbon and hydrogen atoms either in chains (polymers) or in rings (benzene). The addition of methyl radicals, nitrogen, oxygen and other new elements provides more complex molecules (acids, alcohols), whose accumulation leads to polymeric structures. The polymer industry has reached a great development exploiting this technology. This simple image of matter construction permitted in the XIX century to establish Organic Chemistry as a mastered scientific discipline. Since then, one can reproduce in laboratories several substances generated in principle only by living entities. Already in 1828, Friedrich Wholer demonstrated this principle by synthesizing urea [8].In order to understand why carbon achieves such an elevated coordination degree; we must study its electronic structure. Carbon occupies the 6th position within the Periodic Table, which provides an electron configuration of $1s^2$ $2s^2$ $2p^2$. Figure 2.9 shows a scheme of the electron distribution in orbital, where the arrows indicate the spin polarization

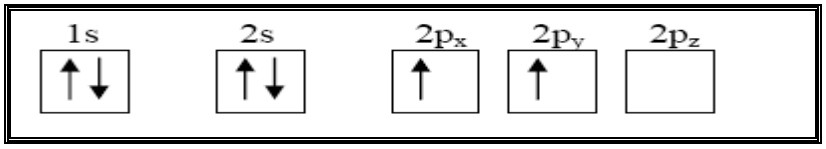

Fig 2.9 Electron distribution in the carbon orbital for a carbon atom

The sub indexes x, y and z indicate symmetry of p orbital with respect to the corresponding axis (Fig.2.10). This differentiation is not required in s orbital, since they are spherical.

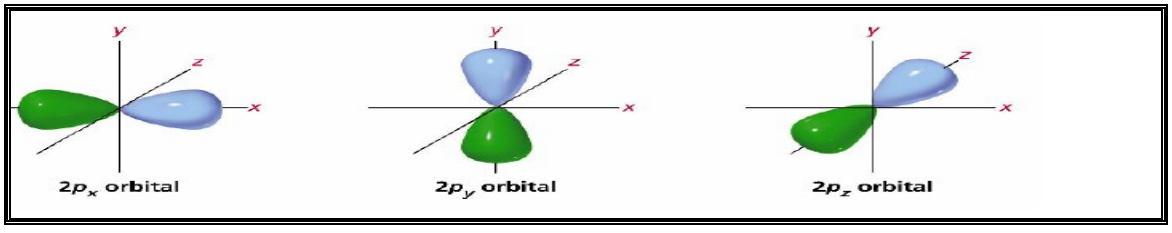

Fig. 2.10 Spatial orientation of the atomic orbital p.

Electronic orbital of the carbon atom contain only two unpaired electrons, behaving thus as bivalent element. In order to justify the tetra valence of carbon, one of the two electrons from the 2s orbital must occupy an empty 2p orbital, resulting in the scheme of Fig. 2.11.

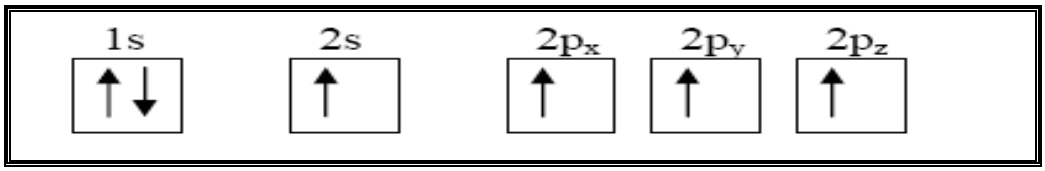

Fig. 2.11Alternative electronic configuration that provides tetravalent carbon atoms.

As a result of the previous redistribution, carbon has four dangling bonds and all the electrons in the outer layer are unpaired. Then, the linear combination of s and p atomic orbital generates the so called hybrid orbital. Hybridization comprises three cases. The s orbital together with one p gives rise to two sp orbital. When two p orbital are added to s. we obtain three sp^2. Finally, the hybridization of all the orbital from the second layer provides four $sp^{3.}$ The generation of the hybrid orbital is depicted in Fig.2.12.

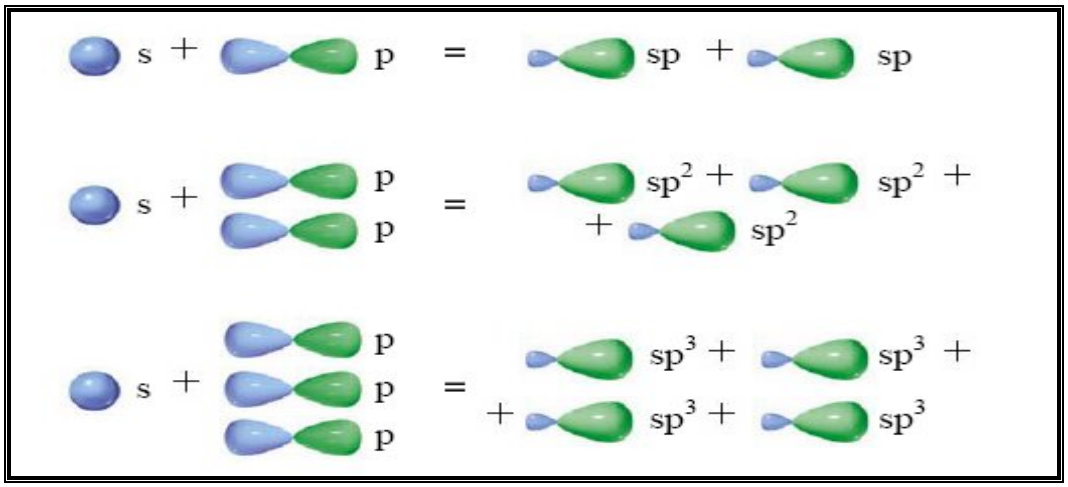

Fig. 2.12 Linear combination of atomic orbital and the resulting hybridizations.

Fig. 2.13 shows the possible geometric configuration in the carbon atom depending of the type of hybridization. Diametrically opposed orientation takes place in the case of sp orbital. In this configuration, both sp orbital make strong frontal σ bonds to an adjacent atom, whereas there are two weak lateral π bonds with neighboring p orbital. On the other hand, trigonal planar

configuration is typical of sp^2, which form σ bonds. The pure p orbital forms a π bond. Finally, sp^3 lobes are oriented towards the vertexes of a regular tetrahedron.

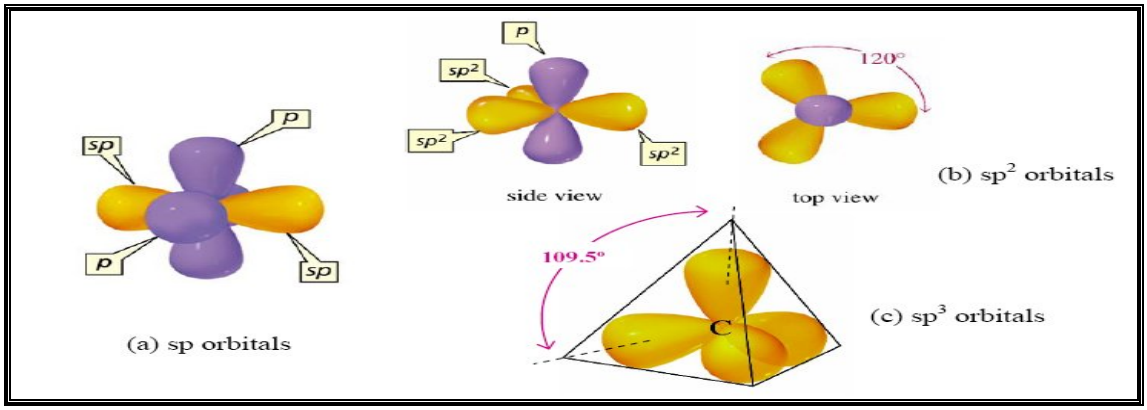

Fig. 2.13 Spatial arrangement of orbital in carbon atom in the case of (a) sp, (b) sp^2 and (c) sp^3 hybridizations.

Carbon presents allotropy, i.e. three different phases have been found in solid state: graphite, diamond and amorphous carbon. They are constituted by carbon atoms bonded by sp^1, sp2, sp^3 and combinations of both hybridizations, respectively. There exists another configuration of carbon: the polymer-like form. It is found when carbon is diluted with Hydrogen and it presents low hardness, high transparency and electrically it behaves as an electric insulator. The spatial distribution of polymeric carbon comprises a rich variety of shapes and lengths, which gives rise to compounds with different chain types. They are divided into open (aliphatic) and closed, being the former lineal or ramified and the latter alicyclic or aromatic.

2.4.2 Graphite

Graphite shows a stable trigonally bonded crystal structure (Fig.2.14). Carbon atoms become bonded by σ bonds due to three superposed sp^2 orbital, adding a π bond that results from the interaction of pure p orbital. This material is soft, optically opaque, chemically active, and is a good electric conductor. The atoms are organized in parallel and single-atom planes, which are called graphenes. Carbon atoms from adjacent planes are bonded by weak dispersion van der Waals forces, which allow two graphenes to slip one on each other and confers special lubricating properties to graphite. The in-plane bond length is 0.142 nm, whereas the inter-plane distance is 0.341 nm. Graphite crystallizes in hexagonal close-packed (h.c.p.) network, and its most important applications are pencil tips, electrodes and solid lubricants.

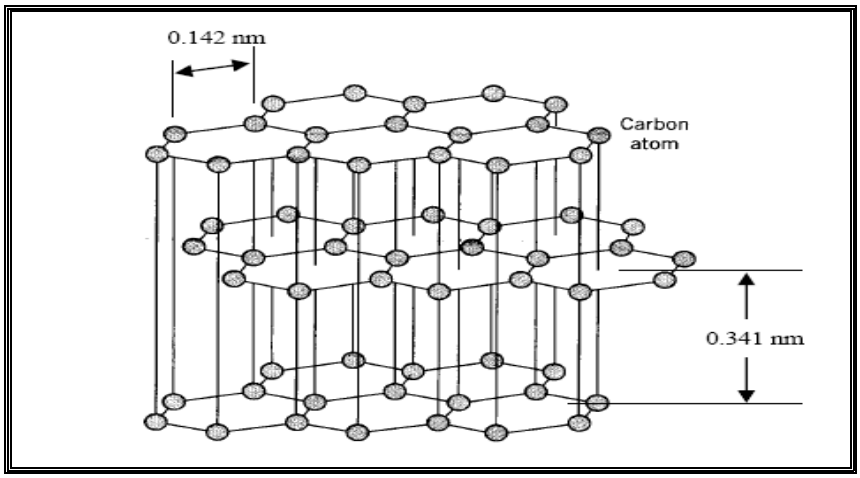

Fig.2.14 Crystalline structure of graphite, showing a portion of three graphenes.

2.4.3 Diamond

Diamond structure results from the metastable tetragonal (σ) bonding of carbon atoms, and is only stable at high pressure and high temperature. It is considered to be a material with various extreme physical properties. First of all, it exhibits the highest elasticity module known to date. In fact, diamond establishes the ultimate hardness limit basically due to the superior strength of its chemical bonds. Complete sp^3 hybridization occurs and, therefore, all atoms become bonded via strong frontal σ bonds. The C-C bond (sp^3) is 0.154 nm long, a bit longer and weaker than that in graphite (sp^2), and its crystallographic structure consists of two superimposed face-centred cubic (f.c.c.) lattices shifted by one-quarter of the cube diagonal (Fig. 2.15).

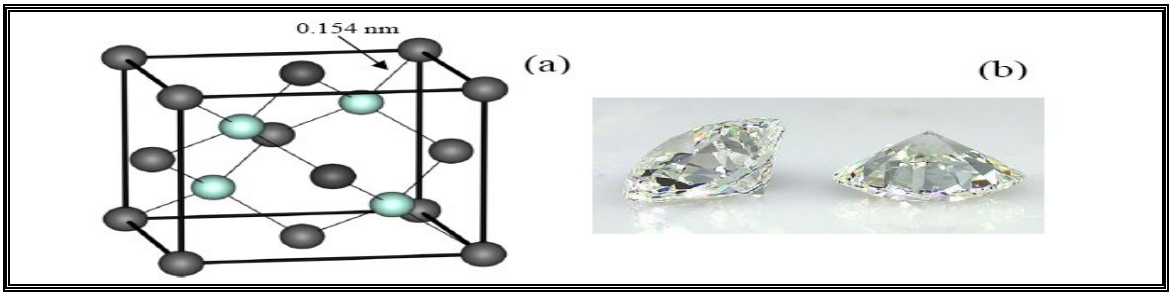

Fig. 2.15 (a) Schematic picture of a diamond lattice and (b) examples of cut diamond gemstones

Such bonds confer the extreme hardness of Diamond and the highest atom density among all Polymeric carbon can also host a great fraction of sp^3 bonds, although the majority of them come from C-H groups and therefore the material is soft. Diamond is mostly employed in cutting tools (edges), abrasive coatings (dust) and jewelers. A prominent use of diamond in electronic applications has taken place due to the interesting properties when the material is chemically doped, especially with the recently discovered superconductivity [9]. Table 2.4.1 provides a list of some applications of diamond along with the required properties.

Table 2.4.1 List of some applications of diamond and the required properties.

Application	Required properties
Ultra hard tool coating	High hardness
Abrasive grain	High hardness
Computer hard disk coating	High hardness, low wear
Watch glasses	High hardness, scratch resistance
Prosthetic coating	High hardness, low wear
Optical coating	High refractive index
Infrared laser windows	Transparency to IR
Semiconductor devises	Large band gap

Diamond conventional preparation requires high-pressure and high-temperature processes (HPHT). Nowadays, thin films of single crystal diamonds in thin film form are prepared by Chemical vapor deposition method at high deposition rates, which opens new perspectives for the diamond applications.

2.4.4 Fullerenes and Nano tubes

Buckminster fullerenes were introduced in 1980s as an additional form of carbon. They were formulated as C_{60}, and consist on spherical lattices formed by 60 sp^2-bonded carbons (Fig. 2.16 a). Extensive research on fullerenes has been undertaken for medical applications using fullerenes as substitutive ligands or in biosensor devices. In the early 1990s, a subset of fullerene science appeared. The preparation of new cylindrical structures called carbon nanotubes was firstly reported by Ijima [1991]. They were called multi-walled nanotubes, since they consisted on multiple graphenes that formed a cylinder surface (Fig.2.16 b). Further refinements permitted the deposition of single-wall nanotubes. Both fullerenes and nanotubes were initially grown by arc discharge and laser ablation techniques, and recently they have been produced by Chemical Vapor Deposition (CVD) method. Most carbon nanotubes applications include field emission devices, fuel cells, cold cathodes and ultrahigh-strength structural materials.

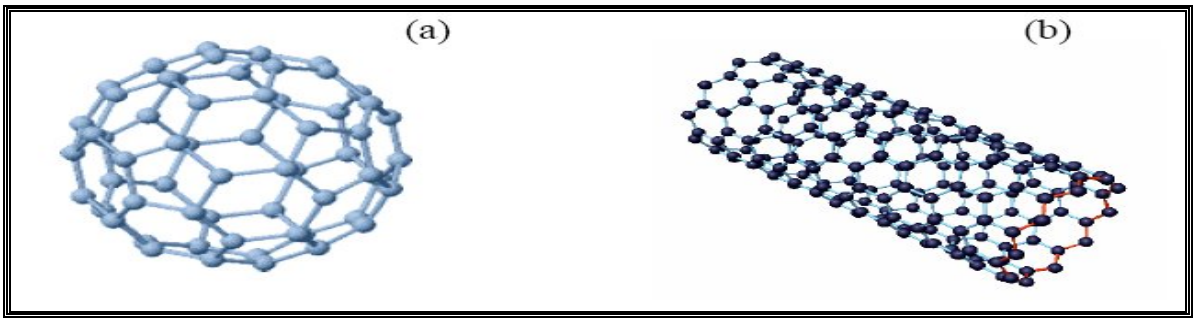

Fig. 2.16 (a) fullerene C_{60} and (b) nanotubes as examples of carbon nanostructures.

2.4.5 Amorphous carbon

Besides diamond and graphite, carbon can form an amorphous phase, which is the nucleus of this thesis. Amorphous carbon (a-C) is obtained under controlled deposition of the amount of diamond, graphite and polymeric phases. Its close relationship with Diamond like carbon (DLC) is analyzed next by citing some key definitions from the International Union of Pure and Applied Chemistry (IUPAC).

Diamond-like carbon (DLC):

Diamond-like carbon (DLC) films are hard, amorphous films with a significant fraction of sp^3-hybridized carbon atoms and which can contain a significant amount of hydrogen or without

hydrogen which are called tetrahedral amorphous carbon (ta-C). Depending on the deposition conditions, these films can be fully amorphous with varying sp^3 content present in the film. These materials are not called diamond unless a full three dimensional crystalline lattice of diamond is proven.

Amorphous carbon:

Amorphous carbon is an allotrope of carbon that does not have any crystalline structure as with all glassy materials "A carbon material without long-range crystalline order. Short range order exists, but with deviations of the interatomic distances and interbonding angles with respect to the graphite lattice as well as to the diamond lattice." Actually, the IUPAC has considered that hard amorphous carbon films and diamond-like carbon films are synonym expressions. In our case, the prepared a-C films have high hardness values and other important properties. From the structural point of view, the short order up to 6-10 atomic distances is synonymous of systems with nanocrystalline structure.

Tetrahedral amorphous carbon (ta-C): amorphous carbon which contain a mixture of sp^2 and sp^3 bonded carbon atom with a very high sp^3 content (>70% maximum upto 90%) interconnected by a high energy covalent bond have a excellent mechanical and electrical properties close to diamond. It is not having any hydrogen but hydrogen incorporated ta-C can also be made by introducing hydrogen gas during deposition of ta-C films.

The Amorphous carbon (DLC) matrix does not contain only one determined hybridization, but contains all three in different proportions. A phase diagram of carbon as a function of sp^2 and sp^3 bonding, and of hydrogen content, is shown in Fig. 2.17. It presents a ternary diagram, where amorphous carbon is understood to be a mixture of the three "pure" phases. There, a-C showing disordered graphitic structure lies in the lower left hand corner, and hydrocarbon polymers are located next to the hydrogen abundant region, where films cannot be deposited. Preparation of a-C containing large sp^3/sp^2 ratio is desirable to obtain "diamond-like" properties. In this way, sputtering and Plasma enhanced chemical vapor deposition (PECVD) increase sp^3 bonding, although the latter technique provides H-rich samples. High plasma density PECVD reactors are necessary to maximize sp^3 bonding and simultaneously diminish hydrogen content. When the sp^3 fraction reaches a high degree, a-C is denoted as amorphous carbon a-C (ta-C) because

tetrahedral bonding due to this hybridization is predominant [10]. The gaps defined between the different phases comprise alloys with intermediate properties.

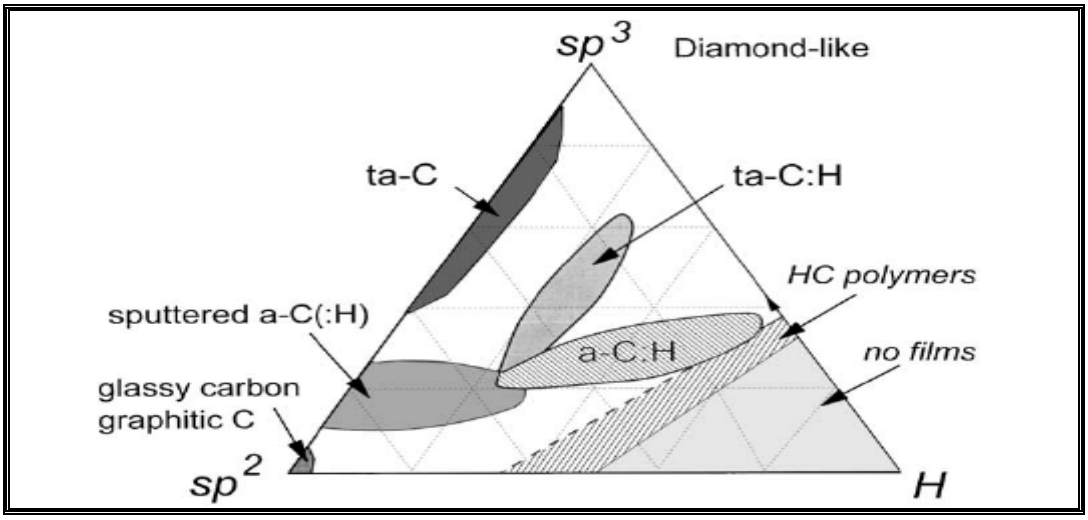

Fig. 2.17 Ternary phase diagram of carbon alloys, as a function of hybridization type

We can imagine the microstructure as a system of covalently bonded carbon atoms organized in a 3-D network, containing a random distribution of sp^2 and sp^3 bonds (Fig. 2.18). This ensures a rich variety of a-C microstructures and properties, and then a classification in sub-categories with common microstructures as presented in Fig. 2.18 is preferred. The high-range correlation disappears by the effect of such spatial randomness and the network becomes globally disordered. Nevertheless, an intermediate range order on the nanometer scale has been found.

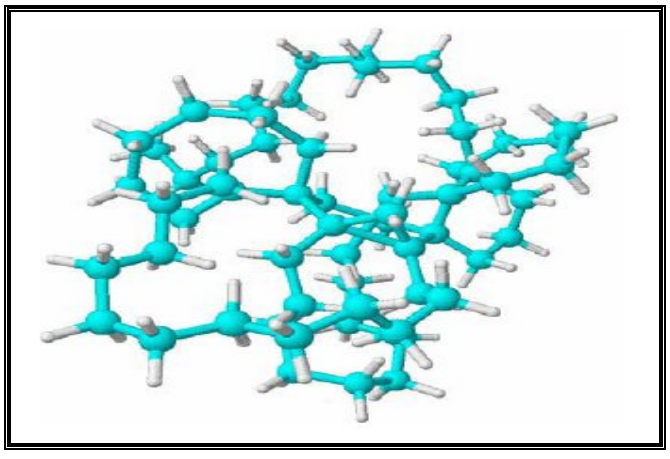

Fig. 2.18 Molecular schematic of high-density amorphous carbon network.

The key parameters to define the disordered structure of DLC are sp^3 fraction, hydrogen content and, in a second term, clustering of sp^2 phase, which takes special relevance in the electronic properties of this material

Nuclear Magnetic Resonance (NMR) and Electron Energy Loss Spectroscopy (EELS) are the most common characterization techniques to derive the sp^3 fraction Mass density is evaluated through X-Ray Reflectivity (XRR) technique and shows a correlation with sp^3 amount. However, the presence of hydrogen complicates this analysis since CHx groups are sp^3 bonded and contribute to a decrease in material density. Visible Raman spectroscopy takes advantage of vibrational properties of the DLC network to determine its sp^3 fraction indirectly and deep UV Raman spectroscopy evaluate sp^3 fraction precisely and supposes one of the most used methods for this task. Fourier Transform Infrared spectroscopy (FTIR) and X-Ray Photoelectron Spectroscopy (XPS) and X-Ray induced Auger electron spectroscopy (XAES) constitute other important tools to study the composition (H content) and bonding structure of amorphous carbon.

Beside the mechanical properties, amorphous carbon is a semiconductor at room temperature that shows remarkable surface and optical properties. It is a chemically and thermally stable material. Table 2.4.2 summaries some important physical parameter of carbon compound or crystalline, including graphite and diamond allotropic forms.

Table 2.4.2 Basic properties of various forms of carbon including Diamond, Graphite, $C_{60,}$ ta-C ,ta-C:H and polyethylene compared to amorphous carbon.

Material	Density (g/cm^3)	Optical band gap(eV)	Hardness (GPa)	Sp^3 (%)	H (%)
Diamond	3.515	5.5	100	100	0
Graphite	2.267	0	-	0	0
Polyethylene	0.92	6.0	0.01	100	67
C_{60}	-	1.6	-	0	0
Glassy carbon	1.3-1.55	0.01	3	0	0
Evaporated C	1.9	0.4-0.7	3	0	0
Sputtered C	2.2	0.5	10	5	0
ta-C	3.1	2.5	80	80-88	0
Hard a-C:H	1.6-2.2	1.1-1.7	10-20	40	30-40
Soft a-C:H	1.2-1.6	1.7-4.0	<10	60	40-50
ta-C:H	2.4	2.0-2.5	50	70	30

2.5 Thin Film Deposition Techniques

2.5.1 Thin film

A thin film is a layer of material ranging from few angstroms (Å) to a few microns (μ) in thickness. There are many applications in the science and industry like optics, electronics, solar energy, infra-red remote sensing etc. Thickness alone is not the criterion of defining a thin film but it is a process by which it should be defined.

Three steps are involved in this process:

1 Creation of material(s) to be deposited in an atomic, molecular or particulate form prior to deposition

2 Transport of material(s) thus created to the substrate in form of a vapor stream or spray etc.

3 Deposition of material on the substrate and film growth by a nucleation and growth process

A thin film formed by screen printing or by spreading paste is not thin film it is a thick film.

2.5.1.1 Mechanical properties

Thin films are unusual specimens for the study of mechanical effects in material. Whatever the application of thin film may be, their mechanical stability and strong adhesion to the substrate are essential qualities. Large internal stresses (10^8 to 10^{10} dyne/cm^2) [1GPa=10^{10} dynes/cm^2] are known to develop in the thin films during their growth. It is sufficient to overcome the film-substrate interfacial adhesion and thus results in peeling off the film if adhesion is only due to physical adsorption. The presence of large stresses is expected to have considerable effect on the mechanical, electronic, magnetic and optical properties of films and it sometimes delaminates the film from substrate.

2.5.1.2 Electronic properties

Electronic properties of thin films have inspired much curiosity and motivated extensive investigations. Depending upon the growth stages, a film may be granular or island-like (that is, consisting of discrete properties) porous (network) or continuous. Each stage has its own characteristic electrical properties and should be considered separately. Electrical conductivity of

granular film is many orders of magnitude smaller than that of the bulk material and is generally characterized by negative temperature coefficient of resistivity. The conductivity is found to vary exponentially with the inverse of temperature, suggesting that the conduction mechanism is thermally activated. It is ohmic at low electric applied field, but nonlinear at high fields. Electrical conduction in porous film is very sensitive to the physical and filamentary bridges brought about by aging, annealing and adsorption. The temperature coefficient of resistance (TCR) of such films is the sum of the metallic, positive and the activated negative (gaps) contributes. Thus a variety of behavior, including a temperature dependent minimum in the resistance is expected.

2.5.1.3 Optical properties

Since the early use of metal films in mirrors and interferometers, interest in the applications of thin metal and dielectric films in optical devices has dominated research in this field. The exploitation of the interference phenomena in this thin films has led to the development of sophisticated multi-layers system with nearly ideal reflection, antireflection, polarization, narrow and wideband reflection and transmission filtering and absorption and emittance properties. Such optical coatings now find routine and indispensable industrial applications in optical instruments.

2.6 Technique for the deposition of thin film

There are several techniques of the thin film deposition which are broadly classified in the following.

(i) physical vapor deposition (PVD)

(ii) chemical vapor deposition (CVD)

2.6.1 Physical vapor deposition (PVD):

Physical vapor deposition techniques are those in which creation of material to be deposited involves a physical process such as (thermal evaporation or sputtering or vacuum arc or laser deposition). PVD methods are clean, dry vacuum deposition methods in which the coating is deposited over the entire object simultaneously, rather than in localized areas. Physical vapor

deposition processes are atomistic where material vaporized from a solid or liquid source is transported as a vapor through a vacuum or low-pressure gaseous or plasma environment. When it contacts the substrate, it condenses. The vaporized material may be an element, alloy or compound. Some PVD processes can be used to deposit films of compound materials (reactive deposition) by the reaction of depositing material with the gas in the deposition environment

Typically, PVD processes are used to deposit films with thicknesses in the range of a few nanometers to thousands of nanometers; however, they can be used to form alloys (e.g., TiN) or with a co-depositing material such as TiC or even a combination of the trilayer coatings, thick deposits and free-standing structures.

The following techniques are covered in PVD.

2.6.1.1 Evaporation

2.6.1.2 Sputtering

2.6.1.3 Vacuum arc evaporation

2.6.1.4 Ion plating

2.6.1.1 Evaporation

Vacuum evaporation Fig.2.19 (thermal including sublimation) is a PVD process where material from a thermal vaporization source reaches the substrate without collision with gas molecules in the space between the source and substrate. The trajectory of the vaporized material is "line-of-sight." Typically, vacuum evaporation takes place in a gas pressure range of 10^{-5} to 10^{-9} Torr, depending on the level of contamination that can be tolerated in the deposited film. For an appreciable deposition rate to be attained, the material vaporized must reach a temperature where its vapor pressure is 10 mTorr or higher. Typical vaporization sources are resistively heated stranded wires, boats or crucibles (for vaporization temperatures below 1,500^{o}C) or high-energy electron beams that are focused and rastered over the surface of the source material (any temperature).

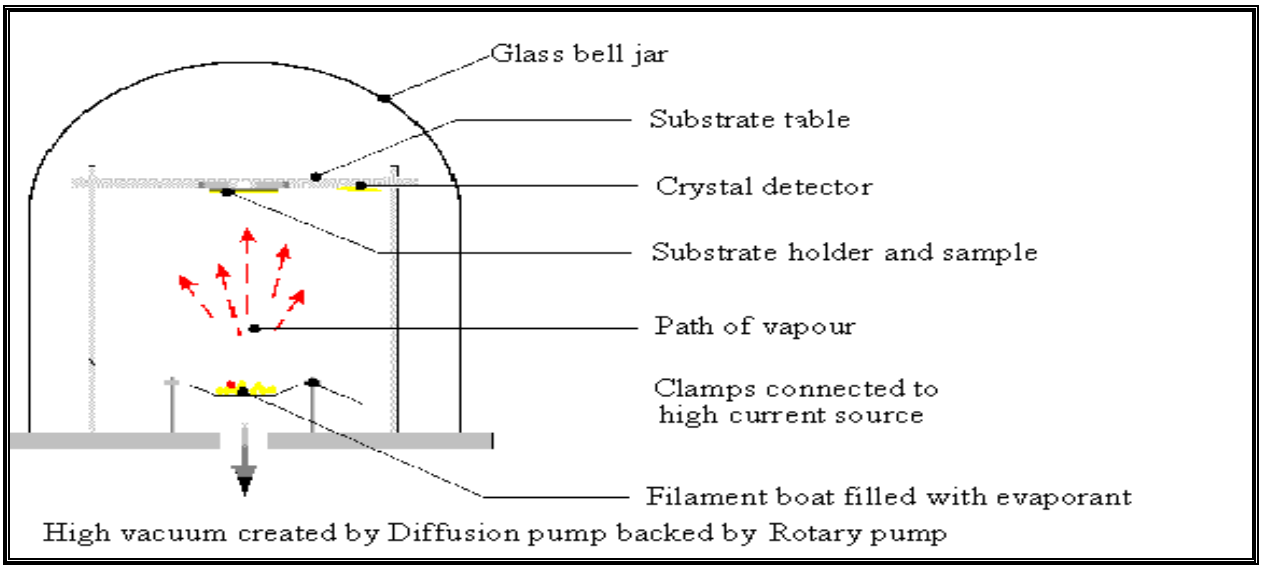

Fig: 2.19 schematics Figure of vacuum evaporation system

This is the first practical thin film deposition technique. The material is created in a vapor form by means of resistive or RF heating. The vapor atoms thus created are transported through vacuum to get deposited on the substrates The evaporant material is supported on a source which is then heated to a sufficiently high temperature(1000 °C – 2000° C) to produce desired vapor pressure(> or = 10^{-2} Torr). The requirements for source material are that it should have a negligible vapor pressure at deposition temperature and should not react with the evaporant.

2.6.1.1.1 Advantages of vacuum evaporation

1. High-purity films can be deposited from high-purity source material.

2. Source of material to be vaporized may be a solid in any form and purity.

3. The line-of-sight trajectory and "limited-area sources" allow the use of masks to define areas of deposition on the substrate and shutters between the source and substrate to prevent deposition when not desired.

4. Deposition rate monitoring and control are relatively easy.

5. It is the least expensive of the PVD processes.

2.6.1.1.2 Disadvantages of vacuum evaporation

1. Many compounds and alloy compositions can only be deposited with difficulty.

2. Line-of-sight and limited-area sources result in poor surface coverage of complex surfaces unless there is proper fixturing and movement.

3. Line-of-sight trajectories and limited-area sources result in poor film-thickness uniformity over large areas without proper fixturing and movement.

4. Few processing variables are available for film property control.

5. High radiant heat loads can exist in the deposition system.

2.6.1.2 Sputtering

Sputtering is a method of depositing both thin metal films and insulators onto a substrate. Unlike evaporation, the material to be sputtered does not have to be heated. The deposition of alloys and insulators as composite materials are two important benefits of sputtering. Sputtering has additional benefits as a deposition technique when compared with evaporation.

In sputtering a solid surface is bombarded with energetic particle, the surface is eroded and surface atom is removed due to collision between surface atoms and the energetic particles. This phenomenon is named sputter or sputtering.

Sputtering as a deposition technique may be described as a sequence of these steps:

When the surface of solid, i.e. Target, is bombarded with argon ions several interactions of ion with the surface are expected as mentioned in the following point.

(i) The incident ions are reflected, probably being neutralized in the process.

(ii) The impact of ion causes the target to eject a secondary electron.

(iii) The ion is buried in the target. This is the phenomena of ion implantation.

(iv)The ion impact causes some structural rearrangements in the in the target material.

(iv) The ion impact sets up a series of collisions between atoms of the target, possibly leading to the ejection of one of these atoms.

(v) This is the phenomena of sputtering.

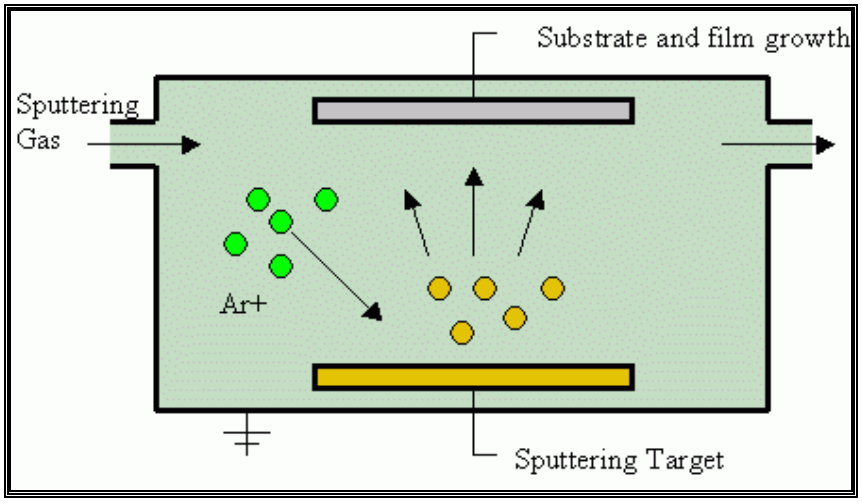

Fig: 2.20 sputtering system

2.6.1.2.1 Mechanism of sputtering

Two theoretical models have been proposed for the sputtering:

(i) The thermal vaporization theory: surface of the target is heated enough to be vaporized due to the impingement of energetic particles.

(ii) The momentum transfer theory: surface atoms of the target are emitted when the kinetic moments of the incident particles are transferred to the target surface atoms.

2.6.1.2.2 Advantages of sputter deposition

(i) The sputtering target provides a stable, long-lived vaporization source.

(ii) Elements alloys and compounds can be sputtered and deposited.

(iii) In some configurations, reactive deposition can be easily accomplished using reactive gaseous species that are activated in plasma (such as TiN in the presence of N_2 gas).

(iv)There is very little radiant heat in the deposition process.

(v) The source and substrate can be spaced close together; deposition chamber can have a small volume.

2.6.1.2.3 Disadvantages of sputter deposition

(i) Sputtering rates are low compared to those that can be attained in thermal evaporation.

(ii) In many configurations, the deposition flux distribution is non-uniform, requiring moving fixturing to obtain films of uniform thickness.

(iii) Sputtering targets are often expensive and material use may be poor.

(iv) Most of the energy incident on the target becomes heat, which must be removed.

(v) In some cases, gaseous contaminants are "activated" in the plasma, making film contamination more of a problem than in vacuum evaporation.

2.6.1.3 Vacuum arc Evaporation

In vacuum arc deposition, the vapor source is vaporized of the cathode or anode. It is a low – voltage high-current electric arc in a good vacuum

2.6.1.3.1 Types of Arc

There are two types of arc: the Cathodic Arc and Anodic Arc.

2.6.1.3.1.1 The cathodic arc

It is a low voltage, high current plasma discharge that takes place between two metallic electrodes in vacuum. The cathodic arc is also called a metal vapor vacuum arc or simply a vacuum arc, but cathodic arcs also occur at elevated gas pressure when the gas participates significantly in the discharge processes.

2.6.1.3.1.2 The Anodic arc

Anodic arc process is quite different from the cathodic arc. Anodic arc is a high current discharge that is sustained at least in part by material evaporating from a hot anode.

We will discuss the cathodic vacuum arc technique in detail in next chapter.

2.6.1.4 Ion Plating

Ion plating refers to processes in which the substrate and the film are exposed to a flux of high energy ions during deposition. This is a combination of evaporation and chemical vapor deposition (CVD) However, there is a sputter etching of the film during growth by these energetic ions and one has to keep the deposition rate faster than the sputter rate The substrate temperature can also be raised which in some case will require the need of subsequent heat treatments

The evaporation of material is done by resistive heating or e-beam heating evaporation and plasma is created by CVD method.

The ion plating has been used to get better film adhesion especially for an incompatible substrate film combination. This technique also gives a better electrical contact for film of Pt, Au on Si. The technique has also been used to deposit films for lubrication, wear resistance and corrosion resistance.

2.6.2 Chemical vapor deposition (CVD)

Chemical vapor deposition (CVD) is a chemical process used to produce high-purity, high-performance solid materials. The process is often used in the semiconductor industry to produce thin films. In a typical CVD process, the wafer or substrate is exposed to one or more volatile precursors, which react and/or decompose on the substrate surface to produce the desired deposit. Frequently, volatile byproducts are also produced, which are removed by gas flow through the reaction chamber. Micro fabrication processes widely use CVD to deposit materials in various forms, including: monocrystalline, polycrystalline, amorphous, and epitaxial.

2.6.2.1 Plasma enhanced chemical vapor deposition (PECVD)

Plasma enhanced chemical vapor deposition (PECVD) is a process is shown in Fig. 2.21 which is mainly to deposit thin film from a gas state (vapor) to a solid state on some substrate. There are some chemical reactions involved in the process which occur after creation of plasma. The plasma is generally created by RF frequency or DC discharge between two electrode where in between the space is filled with the reacting gases.

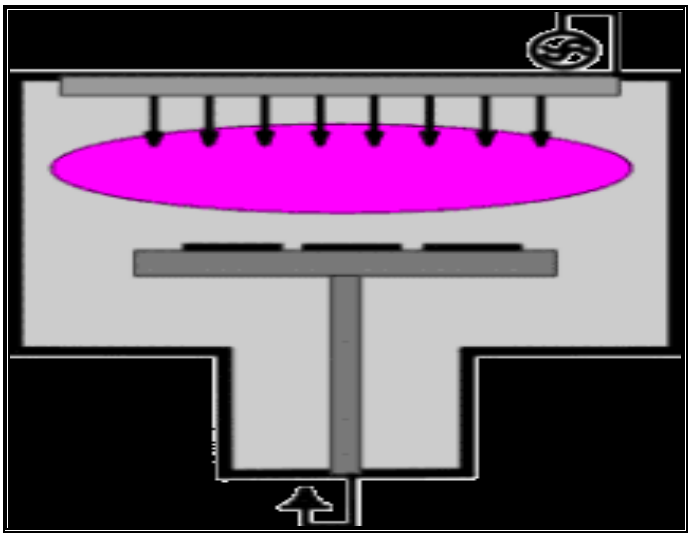

Fig: 2.21 schematic diagram of PECVD method

2.6.2.1.1 Advantages of plasma-enhanced CVD

(i) Many elemental, alloy, glassy and compound materials can be deposited.

(ii) The microstructure of the material can be varied over a large range, sometimes from amorphous to polycrystalline to single crystal.

(ii) High deposition rates.

(iv)Complex surfaces can be coated uniformly.

(v) Equipment is compatible with other vacuum processes.

2.6.2.1.2 Disadvantages of plasma-enhanced CVD

(i) High deposition temperatures are usually required for complete decomposition or reaction.

(ii) Some precursor material may be expensive, dangerous or unstable.

(iii) Processing gases and vapors and by-products must be disposed of by the pumping system.

(iv)There are many processing variables such as vapor concentration, gas composition, heating profile and gas flow pattern.

(v) Incomplete decomposition of the precursors can leave undesirable impurities in the deposited material.

CHAPTER 3

FILTERED CATHODIC VACUUM ARC (FCVA) TECHNIQUE

Introduction

Vacuum arc is a low voltage and high current plasma discharge between two metallic electrodes in vacuum. It also emits macroparticles and neutrals along with the ions. The electrode material itself is used to sustain the discharge without need for a background gas and the process can therefore occur under vacuum conditions. When the plasma material is emitted from the cathode surface the term 'cathodic vacuum arc' is used. This technique is widely used for hard, wear resistance coating on cutting and forming tools, corrosion resistance and decorative coating on door knobs, shower head, artificial jewelers and many other substrate. Most of the solids in the periodic table can be deposited by the cathodic arc deposition.

3.1 Brief history of conventional vacuum arc:

The vacuum arc is a low voltage, high current plasma discharge that takes place between two metallic electrodes in vacuum. The idea of generating coatings by a vacuum arc was first suggested by **Thomas Edison** and he was awarded a patent on arc plasma deposition, in 1892[11]. In the last few decades, the development of vacuum arc was carried out by the scientists worldwide for applications as a deposition tool for thin films. For example, Electrical properties of these vacuum arc produced carbon films were reported by **Blue and Danielson** in 1956[13], Other kinds of metallic and hard coatings were conducted in the 1960s by several research groups worldwide, such as **Wolter** and **Lucas** et al.[14] . The first ''modern'' study of the properties of metal coatings deposited from vacuum arc began in 1965 **by Kikushi** et al.[14.] From there on, many research groups progressively continued work to understand the cathodic arc and plasma processes, with direct applications in the deposition of hard coatings. In the middle of 1970s, the scientists from the Soviet Union engaged in this field of research expanded the applications by reactive deposition of nitrides. Various arc sources were patented in 1970s and 1980s, such as arc vaporization sources by **Sablev** et al. in 1970[15] and **Snaper** in 1974[16]. The potential application of vacuum arc in industry was concerned with parts for tractors and industrial machines, and was first published in 1970, the development of vacuum arc

deposition equipment intensified in the 1980s. Currently there are many small and large companies engaging in the utilizing or setting-up of cathodic vacuum arc equipments

3.2 Principles of vacuum arc technique

When the arc is triggered by a striker (mechanically, electronically and electro-mechanically) the current is concentrated at a small number of discrete sites called cathode spot as shown in Fig 3.1. These cathodic spots are an intense source of electrons, metal atoms and micron - sized droplets of cathode material with extremely high current density, power density and plasma density (Fig. 3.2 shows the photograph of arcing in a cathodic vacuum arc). The formation of cathode spots is a fundamental characteristic of the vacuum arc discharge, which moves across the surface of the cathode randomly in the absence of external magnetic/electric fields. The time constant of the cathode spot is in the sub-microsecond range and the size is mostly of the order of a micron, depending on the material and surface conditions.

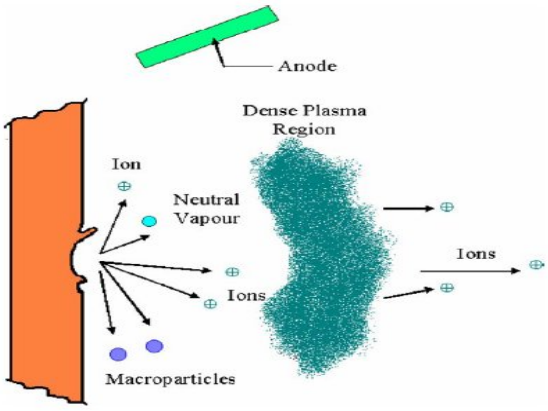

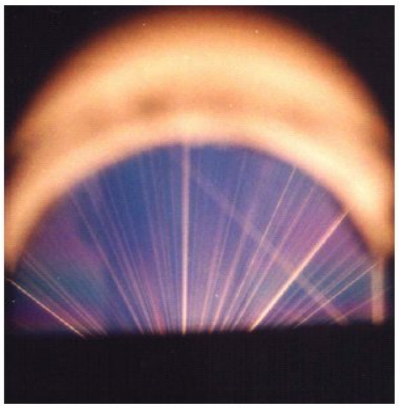

Fig 3.1. Cathodic arc spot with the generation of plasma. **Fig. 3.2. Image of arcing in a cathodic vacuum arc**

The vacuum arc plasma is produced at non-stationary cathodic spots with very high current density of order 10^6 to 10^8 A/cm^2. The high current density is associated with an extremely high power density of order 10^{13} W/m^2 to provide the conditions for the localized phase transformation from the solid cathode material to fully ionized plasma. The high plasma density

is of order of 10^{20} to 10^{21} m^{-3} in vicinity of the cathode and quickly decreases to 10^{17} to 10^{18} m^{-3}, as the distance increases from the cathode spot .The plasma expands from the cathode spots into the vacuum, and in an ion source embodiment, streams toward the ion extractor system. The plasma expansion has been studied theoretically in terms of a free-boundary plasma jet. Plasma production and electron emission at cathode spots are essential for the operation of vacuum arc discharges as they enable current transport between cathode and anode. Plasma parameters are normally obtained by averaging over many individual measurements

Arc burning voltage during discharge is mostly found below 30 V (in the range of 15-30V) and varies according to the cathode material .The formation of energetic ion beams from a plasma by a set of extractor electrodes is more or less well understood for the case when the plasma is drift free, i.e., when the ion drift velocity is small compared to the ion acoustic speed. Most kinds of plasmas are created drift free, and the usual scenario for ion beam formation prevails.

The metal plasma generated at the cathode spots expands rapidly from the cathode into the vacuum ambient with supersonic ion velocities in the range 1 x 10^4 to 3x10^4 m/s with respect to the ion sound velocity. The range of the ion velocity corresponds to ion energy of about 18–160 eV depending on the cathode material as well as their ion mass, which has been determined largely due to the electron-ion coupling. These high ion energies are one of the important features of cathodic vacuum arc and it is critically important to the materials properties of the film deposited. The high deposition energy of the condensing atoms provides a kind of pseudo temperature to the growing film, which in turn favors surface atom mobility and promotes adhesion and thus results in high film quality. The physical phenomena involved here are similar to ion Beam assisted deposition (IBAD). By the control of ion energy, such as the applying of substrate bias, the film morphology and structure can be optimized.

In addition to the high ion energy, high ionization and multiple ion charge states are also the most interesting properties of the vacuum arc process, which are strongly dependent on the materials of the cathode. The cathode material in the plasma is normally fully ionized and it allows the formation of relatively high fraction of multiple-charged ions.

The distribution of the ion charge states could be influenced by magnetic fields, current transients, or input power through varying the arc burning voltage. The ion were generally

multiple charge state ranging from 1^+ up to 6^+, depending on the metal species, the mean ion charge state is between 2^+ and 3^+ typically higher for materials with high melting point. It had been found that ion charge states could be enhanced by use of high arc current, up to kilo ampere range, an effect that has been attributed to the magnetic field of the arc current itself .However, the ion charge states were totally independent for low current vacuum arc processes, within the range of 50–300 A . One way to enhance ion charge states is to form the arc discharge in a vacuum arc ion source by the application of a magnetic field of adequate strength, generally greater than about 0.1 T (1000 Gauss). It had been shown that ion charge state distributions of vacuum arc ion sources were associated with the arc operating voltage. The enhancement of the ion charges could be achieved by increasing the arc voltage utilizing the transient processes that accompany an arc current spike. At the beginning of each arc pulse, ion charge states could be enhanced by approaching asymptotically steady-state values with pulse duration longer than 100 μs. At the end of each arc pulse, the reduced ion charge states were partially ascribed to the charge state-dependent ion drift time in the pre-extraction plasma expansion zone and to a decrease of the electron temperature.

3.3 Current magnetic filters incorporating cathodic vacuum arc

3.3.1 Filtering of macro particles

Various techniques and devices have been employed to reduce the presence of macro particles in the films. Generally, the simplest method of reducing the number of macro particles in the condensing film is to take advantage of the spatial distribution of the macro particle emission and place the substrate in the deposition chamber. However, the substrate must not be in the direct line-of-sight of the cathode. Brandolf [17] has proposed the use of a shield which is placed between the substrate and arc source. The substrate and shield are then biased to attract the plasma around the shield and onto the substrate. The macro particles are trapped on the front of the shield and do not impinge on the substrate. Although macro particles have been observed to decrease using this technique, but the main disadvantage is the low deposition rate.

Another method of reducing macro particles is based on magnetic steering, where the movement of the cathode spot on the cathode surface can be controlled by the use of ‘‘internal’’ magnetic

fields (e.g. fields that are applied directly behind the cathode itself) or ‘‘external’’ fields (e.g. a magnetic solenoid mounted directly in front of the cathode). The best results have been achieved by using curved magnetic ducts to separate plasma from particles basing on the indirect trajectories between cathode and substrates. Furthermore, there are many modifications incorporated into the magnetic ducts, such as baffles, etc. and these modifications have been proven to improve the filtering performance. In this situation, improvement in filtering performance refers to high transmission of a plasma beam with little or no macro particles reaching the substrates. Its attraction is promising primarily due to its capability of producing high quality metal and compound films at practical rates.

3.3.2 Principle of magnetic filters

The magnetic filter was first demonstrated by Aksenov et al.,[18] proving that neutrals and macroparticles could be filtered out from an arc source by using a toroidal filtered duct. The basic idea is to guide the plasma by a curved magnetic field to the substrate which is located just beyond the line-of- sight of the cathode. Macroparticles may be slightly charged but the mass-to-charge ratio is vastly greater than the corresponding ratio for electrons and ions, and therefore macro particles move along almost straight or line-of-sight trajectories due to their inertia. Macro particles will be separated from the plasma and thus removed through magnetic filtering. For liquid macroparticles, they may hit the filter wall and adsorbed onto it, thus removed from the plasma flux. Solid macro particles might also adsorb onto the wall but it was more likely to be elastically reflected. Most of the reflected macro particles would be caught in baffles but statistically, but some of them would still be found in the deposited films. A macro particle-trapping filter wall could be used to solve this problem of ‘‘bouncing’’ macro particles and had been shown to reduce embedded macro particles significantly.

In the presence of an axial magnetic field, the motions of electrons and ions inside the plasma are quite different. The electrons spiral around the field lines until they collided with another particle. Electrons travel in a direction which follows the curvature of the solenoid due to their motions bound to magnetic field lines. However, the gyration radii of the electrons are much smaller than those of ions under the same magnetic field conditions. It is obvious that the influence of magnetic field on the ions is less than that of the electrons. Ions will pass through

the filter by following the magnetic field lines due to the electric fields between electrons and ions.

3.3.3 Types of magnetic filters

In the filtered cathodic vacuum arc deposition technique various magnetic filter have been used. In general, magnetic macroparticle filters can be divided in two categories with their architecture (i) closed (ii) open.

Closed-architecture filters are characterized by an enclosure, the 'duct', which is surrounded by magnetic field coils. Macroparticles are expected to stick to the duct wall or to be trapped by baffles placed inside the duct. For open filters, macroparticles fly away the region of plasma transport through the solenoid's turns without sticking to walls due to the 'free-standing' magnetic field coil without duct. DC-Operated filtered cathodic vacuum arc (FCVA) is usually designed using closed-architecture filters, while open-architecture filters are preferred for use in pulsed-operated FCVA. Currently, most filters in industrial application.

3.4 Cathodic arc components

Modern practical cathodic vacuum arcs consist of several essential components; a conductive cathode from which the plasma is derived; an anode, which is essentially an electron-collecting electrode; a trigger to initiate the discharge; a power supply; and a vacuum chamber (Fig. 3.3). Additional components may include magnetic confinement coils and a macroparticle filter.

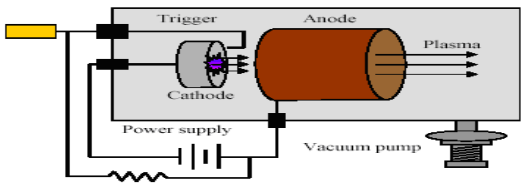

Fig 3.3 :Schematics diagram of the essantial component of cathodic vacuum arc.

Cathode is cooled by a direct water contact to back side and a water-cooled cylindrical anode. Triggering of vacuum arc is an important concern depending on the parameters and operational mode of the source involved triggering can be done electronically ,electro-mechanically or purely mechanically, and it can be laser initiated gas initiated or surface breakdown initiated .Choice of a cathode material is limited only by its ability to conduct a current. All pure metallic species as well as conductive alloys, graphitic carbon and doped semiconductors are potential cathodes. Un-doped semiconductors can also be heated to increase the carrier electron concentration. It is the cathode material that determines the composition of the plasma. Cathode designs are almost invariably a solid disc with one end connected to the power supply and the other circular surface. The anode must be immersed in the plasma plume that originates from the cathode surface. The location of the anode must be such that it does not impede the flow of the majority of the plasma, whilst being close enough to the region of plasma production to collect enough electrons to sustain the discharge. Common anode designs include a cylinder around the cathode through which the majority of plasma can flow, or a flat collecting plate with a central hole that allows the majority of plasma to pass through.

DC and pulsed arcs require different power supplies. DC arcs generally utilize a continuous current source similar to a welding power supply. Pulsed arcs require high instantaneous currents and often utilize a capacitor bank as a power reservoir. One of the limiting factors of the pulsed arc repetition rate is the charging time of the capacitors. A more severe limitation is the resistive heating load of the electrical components. The cooling capability requirement is generally the major limitation in total power usage for both classes of arc. Since the erosion rate of the cathode is closely linked with the power dissipated in the cathode, the plasma production capability of cathodic arcs is in part limited by the ability to cool the electrical components. DC system are capable of very high deposition rate, all commercially used cathodic arc system operate in the DC mode. The pulsed system has a relatively small deposition rate due to their duty factor

$$\mathbf{R\ pulsed = \delta\ R_{dc} \quad ……..(3.1)}$$

Where duty factor is defined $\delta = t_{on}/t_{on}+t_{off}$ by the ratio of the arc on time to the duration of the pulse cycle.

The advantage of the pulsed operation is mainly related to the significantly reduced requirement of cooling because the average power can be kept low (less than 1 kW). Pulsed operation can be desirable for other reason the film property and their controllability can be enhanced by using the pulsed mode. For instance, an a-C film deposited by pulsed cathodic vacuum arc tends to have slightly higher sp^3 content than their DC deposited counter parts. However pulsed operation does not always lead to enhanced properties .Most importantly; many metal films produced by pulsed deposition will allow duty factor exhibit the usually unwanted incorporation of oxygen and hydrogen.

3.5 Cathode Spots

Unlike conventional glow discharges, in a vacuum arc the current continuity at the cathode cannot be provided by the charged particles from the plasma column. At the cathode surface the arc current is channeled through micrometer diameter bright spots called cathode spots Fig. 3.4.These spots have an extremely high current density which is of the order of 10^6-10^8 A/cm^2 that leads to enhanced ionization and energy transfer to the electrode. Energetic ions and electrons are emitted from the spot and provide the metal vapor necessary to sustain the spot are formed by an explosive emission process and the life time of an individual spot at a fixed location has been put at from about 10ns to about a microsecond .The associated areal power density is of the order of 10^9 W/cm^2.The spot size is estimated to be in range 1-10 micron. In addition to production of the plasma species, macroparticles are produced by local heating and explosive emission of molten droplets from the spot region.

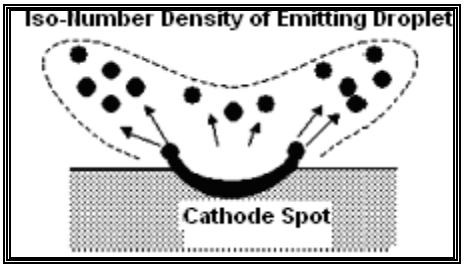

Fig.3.4 Schematic of cathode spot

3.5.1 Current per spot

The current per spot is fairly constant for a given cathode material in vacuum. If the arc current is varied, spots are observed to split or extinguish to maintain this parameter. There is a large variation in the average current per spot for different materials, from around half an amp for solid mercury to a few hundred amps for carbon and tungsten The burning voltage also varies for different materials but is confined to a much smaller range, from 16-25V.Surface contaminants reduce the burning voltage by about 3-5V.

3.5.2 Current density

The current density in an arc spot is extremely high. Measurement of the current per spot can be performed quite accurately. In contrast, estimates of the active area of the spot are difficult and subject to large uncertainties. Visual observations of the spots by high speed camera is subject to errors arising from accurate determination of the active area, as distinct from the luminous area which may be in part ascribed to conductive heating. Additionally, the expanding plasma emits an intense optical signal that can distort the estimates of the spot diameter. Estimates of the spot dimensions by post-arc observations of the arc craters by electron microscopy are also prone to errors. Whilst, it is relatively straightforward to measure the area of damage on the cathode surface, exactly how much of the damaged area was the conduit for the current is difficult to determine due to the explosive ejection of molten material from the spot during the arc. Because of these uncertainties, experimental estimates of the arc current densities range from 10^{9} to 10^{12} $A.m^{-2}$. Theoretical models suggest that the density may be an order of magnitude higher.

3.5.3 Ion velocities

As a result of the high currents and plasma densities, a feature of vacuum arcs is there relatively high kinetic energy imparted to the plasma ions. The very high plasma density creates strong pressure gradients which, combined with high local electric Fields, because the acceleration of ions to supersonic drift speeds. Ion velocities range from 0.5 - 2 x 10^{4} ms^{-2}, almost independent of ion mass and charge state. This provides a unique condition for depositing thin films, affecting the film stress and hardness by imparting energy to the growing film through ion impacts. Additional energy can be given to the ions by applying a potential to the substrate, making use of

the high degree of ionization in the cathodic arc plasma, for example by plasma immersion ion implantation.

3.5.4 Ion Charge States

During the discharge the majority of the plasma atoms are ionized and the ion-to electron ratio is usually limited to around 0.1 at distances greater than a few millimeters from the cathode, Due to the extremely high current densities the material ejected from the spot region contains energetic ions with charge states up to six .Most metal species, at low arc currents, have an average ion charge state of between 1 and 3. It has been observed that external magnetic fields affect the distributions of charge states. High arc currents (>1kA) have also been shown to increase the average charge state. These two effects can be related by considering that an increased arc current results in the production of multiple arc spots. Being a conduit for a large current, each arc spot is the source of a large magnetic field that acts on surrounding spots in the same way as an externally applied field, thereby affecting the charge state proportions. In addition, the average ion charge state during the discharge decreases from an initial maximum to a steady state after around 100μs .This is likely to be due to surface contaminants and adsorbed gases affecting the electronic properties of the cathode surface.

3.5.5 Retrograde motion

The most complicated problem in the vacuum arc technique is the motion of the cathode spot especially in the presence of external magnetic field. The cathode spot move randomly in the absence of the magnetic field but the problem become complicated when we apply external magnetic field. Single cathode spots in the absence of externally applied fields exhibit a random motion across the cathode surface. Spot behavior in the presence of an externally applied magnetic field is somewhat more complicated.

Electromagnetic theory predicts that an electric current density (**J)** in the presence of a magnetic flux density(**B)** is subject to a force, **J** x **B**. In contrast, when observed in an external magnetic field parallel to the surface of the cathode (transverse magnetic field), cathode spots move in a direction opposite to that predicted by the theory. This phenomenon is termed “retrograde

motion". Retrograde motion has been shown to be influenced by the gas pressure in the vacuum chamber. As the background pressure increases, retrograde motion slows, and then reverses at a critical pressure. The inability of the plasma to expand under the forces exerted from the cathode spot below causes the confinement to become unstable and jets of plasma are emitted toward the retrograde side at velocities of $5kms^{-1}$ on average.

3.6 Filtered cathodic vacuum arc as a deposition technique (FCVA)

A Filtered cathodic vacuum arc (FCVA) system is able to deposit films with very little macroparticles. The intrinsic energies of the depositing metal species are sufficiently high that columnar growth is suppressed and self densification of the film occurs, this eliminates the need for substrate heating. The intense ion flux also favors high deposition rates. The kinetic energy of the ions incident on the substrate can be varied by applying a bias on the substrate. The FCVA system is also able to deposit uniform large area coatings, with a carefully designed rastering and control of the ion beam (plasma). Compared with other techniques, such as chemical vapor deposition, spray pyrolysis, and atomic layer deposition, the FCVA does not have any contamination from the original material source. The process of FCVA is based on ion beam deposition, which is not a complex process with an added advantage of having no by products deposited on the substrates. Besides, the source materials used are inorganic, and thus the possibility having waste toxic materials as by-reactants is very low.

The properties of the thin films deposited by conventional physical vapor deposition techniques are frequently inferior to those of the bulk material. The films may have a low packing density, low micro hardness and in many instances, poor adhesion to the substrate. Many of these shortcomings are a direct consequence of the energy of the depositing atoms arriving at the substrate during film growth. The resulting film porosity gives rise to a reduction in mechanical strength, and in the case of dielectric optical films, a reduction in the refractive index. The situation is improved strongly when the energy of the arriving atoms increases directly (e.g. by sputtering rather than thermal evaporation), or indirectly (by bombarding the growing film with more energetic particles). For the FCVA, the high kinetic energy of deposition species eliminates above problem. The FCVA produces coatings with superior characteristics including excellent adhesion and high density as a result of the high intrinsic energy of the depositing ions, which is greater than the minimum displacement energy of the material. This technique is currently well

established as a powerful, cost effective ion-based technique for the deposition of a wide range of metals, alloys, and compounds. Now a days vacuum arc based techniques are used for the deposition of coating materials for variety of applications.

The formation of high energy ions from the cathode material is one of important advantages of the cathodic arc process. This is in contrast to other physical vapor deposition techniques, such as magnetron sputtering and electron beam evaporation, where the distribution of deposition atoms forming the coating is primarily neutral. In many cases, the ions generated by the cathodic arc are multiply charged and with a near optimal kinetic energy for forming dense and adherent coatings on complex shapes. The high degree of ionization in the plasma (usually close to 100%) means that the impact energy of the depositing ions at the growth surface can be readily controlled using electric fields. For example, by adding bias voltage on the substrate, the energy of deposition species could be increased and thus the film morphology and structure can be optimized. During the last decade, many efforts have been made to improve the performance of the off-plane double bend FCVA. In order for the deposition chamber to achieve high vacuum consistently, another load-lock chamber is added. In addition to having a more efficient substrate transport mechanism, this intermediate chamber is a stand alone system which includes an ion beam etching facility for substrate cleaning. This is particularly beneficial for commercial or industry applications. Both deposition process and growth parameters are monitored and controlled by the designed software program. Depending on the exact applications, the system could optimize the deposited film's quality through independent control of cathode composition, substrate temperature, chamber pressure, process gas flow rates, and substrate bias. Film uniformity and deposited area are realized by magnetic scanning system placed at the plasma exit from the filtered duct. The focused beam spot is steered by the variable 2D magnetic scanning field controlled by this program, which allows researchers to obtain thin films with excellent thickness control (-2%) over large substrate area (up to 800 diameter).

3.7 Cleaning of substrate surface

Surfaces exposed to the atmosphere are generally contaminated. Any unwanted material on a surface is regarded as a contaminant. Any manipulation at all contributes to the generation of contaminations. Surface contamination can be gaseous, liquid or solid in its physical state and may be present as a film or in particulate form. Furthermore, it may be ionic or covalent and

inorganic in its chemical character. It can originate from a number of sources, and the first contamination is often a part of the creating the surface itself. Adsorption phenomena, chemical reactions, leaching and drying procedures, mechanical treatment, as well as diffusion and segregation processes can give rise to various composition of surface contamination. So, before a surface can be coated with thin films, it must be clean. If it is not clean, then the film will not adhere well or may not adhere at all. Therefore, the cleaning of surfaces is a very important but also a very difficult and delicate operation. The adhesive forces holding small particles onto surface may be quite strong in terms of bond strength per unit area. The mechanical energy available to break such bonds is relatively small is most cleaning processes. Consequently, in a given cleaning process, a strong effort is needed to reduce the adhesive bonds between contaminant and surface as much as possible.

3.8 Cleaning procedure

Cleaned surface can be classified into two categories: atomically clean surfaces and technological clean surfaces. Surface of the category can only be realized in ultra high vacuum. Practical coating applications require only technologically clean or slightly better qualities of surface. The degree of surface cleanliness must meet the following two criteria: it must be good enough for subsequent processing and it must be sufficient to ensure further reliability of the product for which that surface will be used. A further distinction must be made between cleaning methods that are applicable in the atmosphere and those that are applicable only in the vacuum. In all cases where handling of the parts and use of solvent is required, cleaning cannot be performed in a vacuum. If cleaning in done in vacuum, e.g. by heating operations and particle bombardment, then this is generally conducted inside the deposition system. The various cleaning procedure can be outlined as follows:

3.8.1 Cleaning with solvent

(i) Rubbing and immersion cleaning

(ii) Ultrasonic cleaning

(iii) Vapor degreasing

(iv)Spray cleaning

3.8.2 Cleaning by Heating and Irradiation

3.8.3 Cleaning in an electric discharge

In the present study, films were deposited on silicon wafers. Before the deposition process, the surface of the substrate was cleaned for proper deposition of a-C on it by the method which can be described as follows:

(i) Substrate is first treated with soap solution in ultrasonic vibrator for 5 min.

(ii) Then it is rinsed by deionized water for 2 min.

(iii) Then it is again treated with deionized water at room temperature in Ultrasonic vibrator for 2 min.

(iv)After this, it is treated with isopropyl alcohol (IPA) at room temperature for 5 min.

(v) Then it is treated with tri chloroethylene 5 min.

(vi)Then it is again treated twice with IPA for 2 min.

(vii) Then it is rinsed with deionized water at room temperature and lastly it is dried with dry nitrogen.

CHAPTER 4

DEPOSITION OF AMORPHOUS CARBON FLIM BY MODIFIED ARC BASED TECHNIQUES AND THEIR CHARACTERIZATION

4.1. Details of deposition of film and FCVA system

The combined use of cathodic vacuum arc and magnetic filters for the removal of macroparticles is called filtered cathodic vacuum arc (FCVA). The FCVA is an unusual method for laboratory and industrial use. The deposition of amorphous carbon films has been carried out using a modified FCVA process. Now in this section, we describe the designing and deposition process of the film by modified FCVA process. The FCVA system consists of three components, arc chamber, linear magnetic filter and deposition chamber. The arc chamber consists of water cooled cathode and a mechanical striker. The linear magnetic filter is energized by using a DC supply and gives 350 magnetic field. This was connected to the exit of the arc chamber. The outlet of the linear magnetic filter was fitted to a vacuum chamber equipped with a turbo molecular pump backed by a rotary pump. The deposition chamber was evacuated to 1 x 10^{-6} mbar prior to the deposition.

4.1.1 Deposition process of a-C films

For the deposition a-C films, the arc was initiated using a mechanical striker (a retractable graphite rod of purity 99.999 % and diameter 7 mm). The cathode target has been made of 99.999% of pure graphite of 50 mm diameter. The deposition has been carried out at 24 V and an arc current of 56 A. The substrate was placed on a sample holder at a distance 32 cm from the cathode. The temperature of the substrate has been kept below 40^{o}C. He gas of high purity was introduced through the cathode and the deposition was carried out at 1.0 x10^{-3} mbar. The arc was sustained for 10 sec and then cooled for 1 min. The repetition of the process was done till the required thickness was obtained.

The vacuum arc deposition method has been modified by creating a He or N2 jet in the vicinity of carbon arc. The confinement of the high pressure gas region to the immediate vicinity of the cathode allows the expansion of a carbon plasma plume away from the cathode and smaller fullerene formed in the gas phase are carried by the plasma plume onto the substrate. Depending on whether the gas is injected through the cathode or the anode, the novel technique will either be termed as “cathodic jet carbon arc” (CJCA) “or anodic jet carbon arc” (AJCA). The arc can be run in DC, AC or pulsed mode. The novel cathodic jet carbon arc (CJCA) has been set up (Fig.4.1) to produce a new form of undoped amorphous carbon thin films having embedded nano particle, and nano tubes.

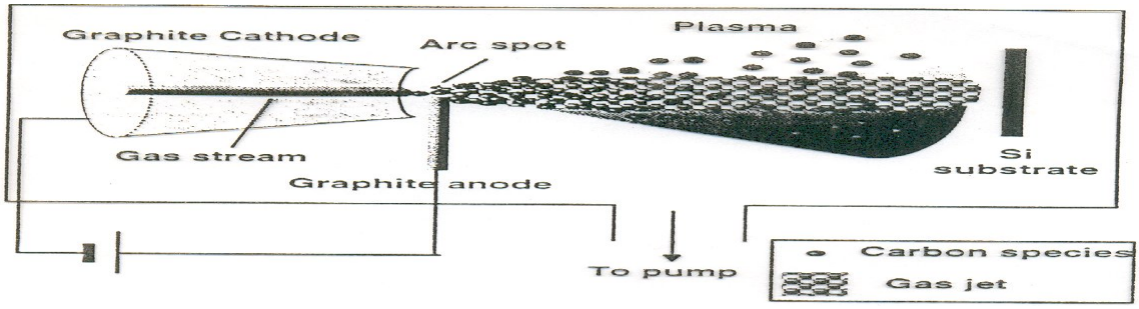

Fig.4.1 Schematic diagram of Cathodic jet carbon arc (CJCA)

4.2 Characterization

4.2.1 Thickness measurement

Thickness of the deposited film is an important parameter, which is required to evaluate the deposition rate and uniformity of the film. A Talystep (Rank Taylor and Hobson, U.K.) profilometer is used for the initial estimation of the thickness of the deposited film. The instrument uses a diamond stylus to measure the height of the step formed on the substrate by suitable means. The corresponding signal gets amplified and will be recorded on magnetic chart paper. The deposition rate was estimated by taking the ratio of the observed thickness of the films to the time of deposition used in depositing these films. The thickness of the film was 1800A^{o}.

4.2.2 X-Ray Diffraction (XRD)

The X-ray diffraction technique (XRD) is the fastest and most convenient method for gross characterization of materials. This technique has been widely employed to examine the microstructure, phase formation, and study of the texture as well as calculation in the lattice parameters. In all X-ray investigations, monochromatized CuKα radiation from a normal focus X-ray tube was used, having wavelengths $\lambda_{K\alpha}$=1.54060Å. For the X-ray study of powders and pellets, the samples were ground using a mortar with a pestle. Peaks were indexed using Bragg's law of $2d_{hkl}\sin\theta_B = n\lambda$, where n is an integer, λ is the radiation wavelength θ_B is the Bragg's diffraction angle and d_{hkl} is the distance between the reflecting parallel planes.

Additional structural information including grain size, strain state, preferred orientation etc can also be ascertained using this technique. The typical XRD curves of a-C films are shown in Fig.4.2.

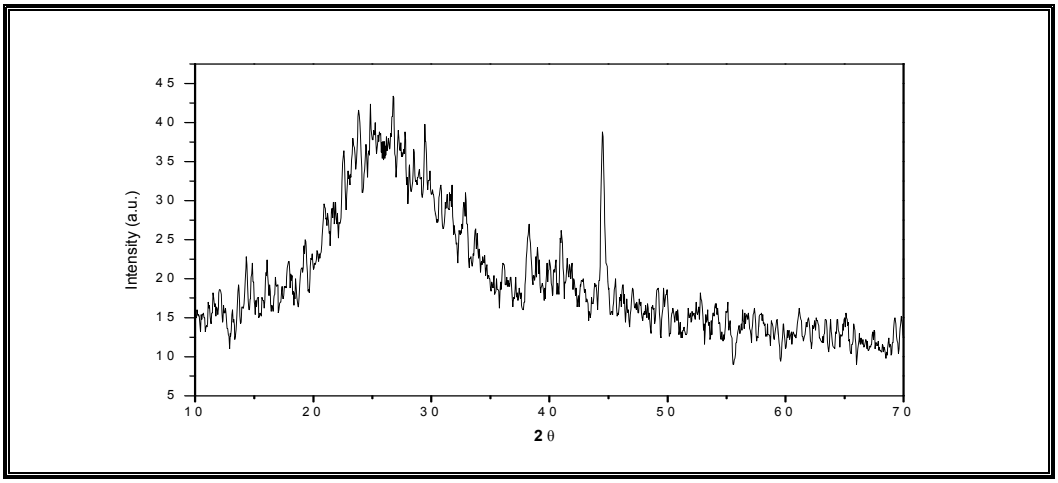

Fig. 4.2

There is a broad peak at around 26^0 which shows the behavior of the amorphous carbon (a-C) film detected by the XRD. The graphical representation of the XRD of the film shows that there is no crystellinity present in the film and therefore it has like an amorphous like structure. There is a sharp peak at 44^0 showing the presence of nanoparticles.

4.2.3 Scanning Electron Microscope (SEM)

SEM is a powerful and versatile analytical technique capable of providing a combination of structural and atomic information at an extremely high spatial resolution. These qualities make SEM an ideal technique for successful characterization of multilayer thin film coatings. SEM provides a detailed investigation into the microstructure, interfaces and elemental composition of the multilayer. It has now become a routine matter to achieve a resolution of around 2 Å.

The working principle of the electron microscope is analogous to that of the optical microscope. The specimen is illuminated by a monochromatic electron beam and a rotated and enlarged image is produced by the objective lens. This image is in turn projected on to a fluorescent screen by means of a combined system of intermediate and projector lenses and can be photographed either on the plate or on the roll film. The diffraction pattern formed at the back focal plane of the objective lens can be projected on to the screen by adjusting the strength of the intermediate lens. Selected area diaphragms (or aperture), which are inserted in the Gaussian image plane of the objective lens, make it possible to record diffraction patterns from particular region.

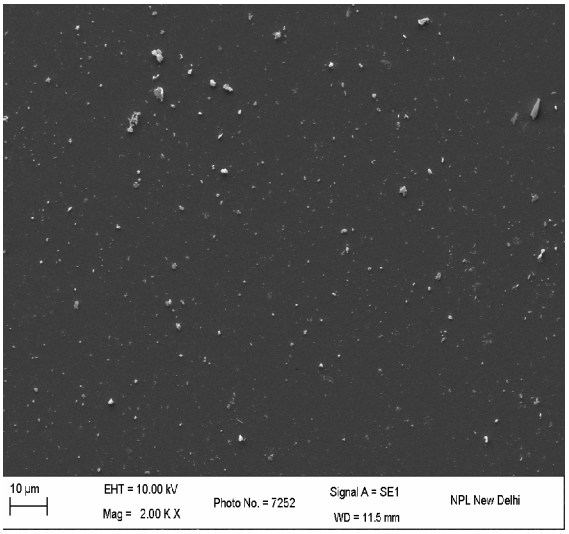

Fig 4.3 (a)

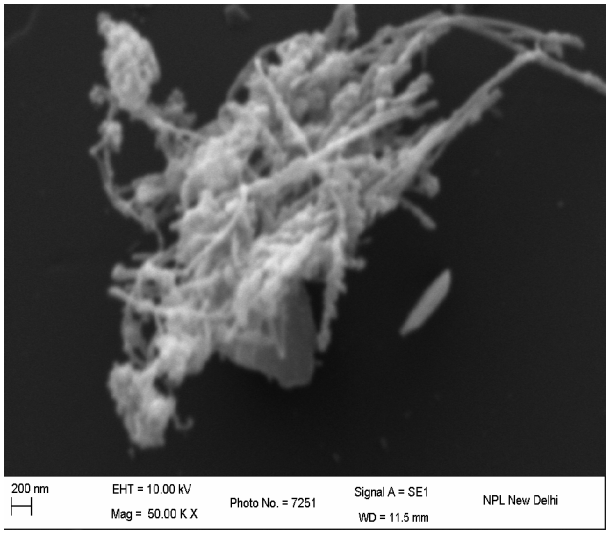

Fig 4.3 (b)

Fig 4.3 (a) shows the amorphous nature of the film with some scattered nanoparticles.

Fig 4.3 (b) shows the presence of nanoparticles nanorods etc. in clusters.

The aim of study using SEM was to see the presence of nano structure and nano particle in the film deposited.

4.2.4 Atomic force microscopy (AFM)

Atomic force microscopy (AFM) or scanning force microscopy (SFM) is a very high-resolution type of scanning probe microscopy, with demonstrated resolution on the order of fractions of a nanometer, more than 1000 times better than the optical diffraction limit. The AFM consists of a cantilever with a sharp tip (probe) at its end that is used to scan the specimen surface. The cantilever is typically silicon or silicon nitride with a tip radius of curvature on the order of nanometers. When the tip is brought into proximity of a sample surface, forces between the tip and the sample lead to a deflection of the cantilever according to Hooke's law.

Mathematically, Hooke's law states that

$$F = -Kx \qquad \text{..... (4.1)}$$

Where $\boldsymbol{x}$ is the displacement of the spring's end from its equilibrium position (a distance, in SI units: metres); $\boldsymbol{F}$ is the restoring force exerted by the spring on that end (in SI units: N or $kg \cdot m \cdot s^{-2}$); and k is a constant called the rate or spring constant (in SI units: $N \cdot m^{-1}$ or $kg \cdot s^{-2}$).

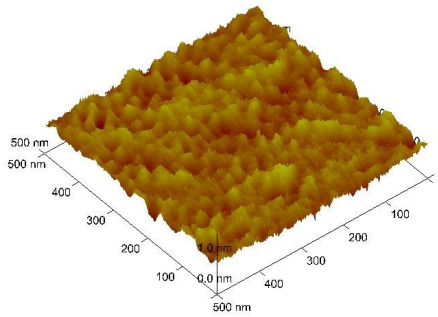

Fig 4.4(a)

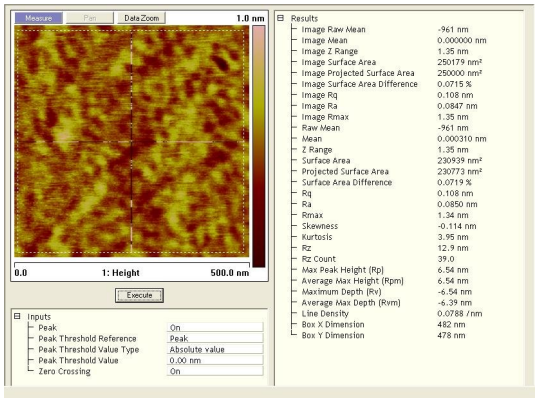

Fig 4.4(b)

The three-dimensional topography of the film is displayed in Fig. 4.4.Atomic force microscopy (AFM) has been used to study surface structures of amorphous carbon (a-C) films. a-C films were prepared by filtered arc deposition (FAD) technique. AFM revealed that the surface on

formed films is uniform and smooth on the nanometer-scale. The average roughness of surface is 0.0850 nm.

4.2.5 Stress measurement

Film deposition can result in a compressive or tensile stress being built up in the coating. The extent of the stress is dependent on a variety of factors, with the most notable including the energy regime of the incident ions or atoms and any lattice mismatch between the substrate and film. The stress in a coating can be determined by measuring the radii of curvature of the substrate before and after deposition using a Tencor surface profiler. The stress σ in the coating is related to the change in radius of curvature by Stoney's equation [19]

$$\sigma = \frac{E t_s^2}{(1-\nu)\, t_f}\left(\frac{1}{R} - \frac{1}{R_0}\right) \qquad \ldots\ldots\ldots (4.2)$$

Where $E_{si=}$ 1.03x 10^{10} N/m^2, is the Young's modulus of the silicon substrate, ν=0.22 is the Poisson's ratio of the silicon substrate and the ratio E/1-ν~180.5 GPa, the substrate and film thickness is represented by t_s and t_f respectively. Finally R and R_0 is the radius of curvature of the coated and uncoated substrate. The radius of Curvature R and R_o of the substrate and the films has been evaluated.

4.2.6 Electrical Conductivity

Conductivity measurements were performed on sample which were made by thermal evaporation in vacuum ~ 10^{-6} Torr on undoped a-C film in a coplanar configuration with a gap of 0.078 cm. These measurements were carried out after annealing at 200^{o}C for an hour in vacuum in the temperature range 30^{o}C to 200^{o}C in the cycle at 5^{o}C. A DC voltage (20V) was applied to the electrodes and the current passing through the film was measured by an electrometer (Keithley Model 610 C). Measurements were carried out under a vacuum of ~10^{-5} mbar. The value of conductivity (σ) was calculated from the relation

$$\sigma = [I \times l] / [V \times b \times t] \text{ ohm}^{-1} \text{ cm}^{-1} \qquad \ldots\ldots\ldots (4.3)$$

Where l is the separation between the coplanar electrodes, b is the width of the electrode, t is the thickness of the film and V and I are the voltage applied and current measured across the coplanar electrode. The value of activation energy (ΔE) is obtained from the slope of the variation of log σ versus 1000/T curve since dark conductivity (σ_D) follows a relation of the form of $\sigma_D = \sigma_0 \exp(-\Delta E/kT)$ ..... (4.4)

Where σo is the conductivity pre exponential factor, k is the Boltzmann's constant and T is the temperature in the Kelvin.

The variation of dark conductivity (σ_D) with the inverse of temperature of as grown a-C films without substrate bias and 350 G magnetic field is shown in Fig.4.5.

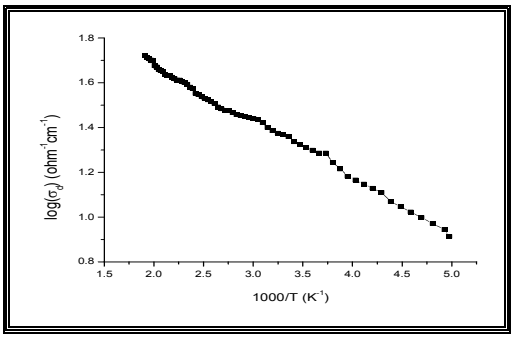

Fig.4.5

It is evident from the Fig.4.5 that the variation of σ_D is a thermally activated process. From the electrical conductivity measurement it is easier to calculate activation energy of the a-C by using expression as

$$\Delta E = kT(\ln(\sigma_0/\sigma_D)) \quad \text{.....(4.5)}$$

The conductivity of the film is found to increase with the increase of temperature. The conductivity of the film is very high of the order~ 10 $ohm^{-1}cm^{-1}$ in comparison to the value reported in literature. The cause of high conductivity may be related to the presence of nano particle.

The table 4.1 summarized the various parameters evaluated from different studies undertaken.

Measured Parameter	Sample (no substrate bias,, magnetic filter 350G)
Thickness	1800 A^o
Stress	3.91 GPa
Deposition rate	9.9 A^0/sec
Conductivity at 30^0 C(σ_D)	10 $ohm^{-1}cm^{-1}$
Activation energy	0.03eV

Table 4.1 Properties of amorphous Carbon (a-C) films.

CHAPTER 5

FIELD EMISSION IN AMORPHOUS CARBON THIN FILM HAVING EMBEDDED NANOPARTICLES FOR POSSIBLE DISPLAY

5.1 History of Field Emission

In 1897, R. W. Wood became the first person to describe the phenomenon of field emission [32], which he observed during experiments with a discharge tube. Initial theoretical insight into this process was provided by W. Schottky in 1923. He assumed that the electrons are emitted over a potential barrier at the surface lowered by the applied electric field [34]. In 1928, R.H. Fowler and L. W. Nordheim developed a theory of field emission based on quantum-mechanical tunneling of electrons through the surface potential barrier [33]. This theory accurately described the dependence of the emission current on the electric field and the work function, which is the energy needed to remove an electron from the Fermi energy level into a vacuum. It also followed from this theory that no external excitation is required for the initiation of this process. A clear evidence to this was obtained by J. E. Henderson et al [35] in their studies of the energy distribution of electrons and the measurements of the calorimetric effect.

An important development in the field emission area was the invention of the field emission microscope by E. W. Muller in 1936 [34]. The understanding of surface properties of field emission has benefited from this invention.

One of the most important results of the quantum-mechanical theory was the prediction of extremely high field emission current densities. In 1940, R. Haefer experimentally proved the feasibility of achieving high current densities of ~106A/cm² [34]. In 1950s, W. P. Dyke and his group achieved current densities of 107-108A/cm² under pulsed and steady-state conditions respectively [36, 37]. A number of important results were obtained by Dyke's group relate to the causes of instabilities and degradation of field emitters. It shows that the main cause of the emitter degradation was Joule heating of the tip by the emission current. M. I. Elinson and co-

workers found that the maximum current values were dependent on the emitter geometry and showed that by increasing the tip cone angle, the current density could be increased by about an order of magnitude without emitter tip damage [34].

Further progress in research on field emission at extremely high current densities had been conducted by G. N. Fursey et al [34]. In DC experiments, thermal effects due to field emission at high current densities were demonstrated. A new type of instability caused by the spontaneous change of the cathode surface micro-geometry near the thermal destruction threshold was discovered. Current densities of 10^9A/cm² were observed with nanosecond range pulse lengths by G. A. Mesyats and G. N. Fursey [34]. Moreover, Current densities of ~10^{11}A/cm² were reported by G. N. Fursey et al, in 1998. These current densities are close to the theoretical supply limit of a metal's conduction band when the electron tunneling probability is unity [34].

Experimental and theoretical studies have been conducted to increase the stability of the field emission current and prevent ion bombardment of the cathode. Recent studies showed that an applied microwave field could reduce the intensity of cathode ion bombardment [34].

The practical applications of field emission began in 1959 by W. P. Dyke whose company produced pulsed X-ray apparatus for recording high-speed processes and compact X-ray sources for medicine [38]. Subsequently, a related phenomenon referred to as explosive emission was discovered [39]. In 1960s, the possibility of using field emitters as an electron sources for atomic-scale resolution electron microscope was demonstrated [40].

The research of using arrays of field emission cathodes in various microelectronic components and devices was suggested by K. R. Shoulders and initiated in the United States by C. A. Spindt [41]. The most striking example of the applications of field emission cathodes to an area of technological interest is in flat-panel displays.

In recent years, with the improvement of the experimental techniques, many new phenomena were observed, for example, broadening of the energy spectra at high current density [42], the presence of additional peak of energy spectra, and the presence of polarized electrons from metallic emitters coated with ferromagnetic films [34]. Although some of these phenomena cannot be explained by previous field emission theories, Fowler-Nordheim model is still the most widely used field emission theory.

5.2 Fowler-Nordheim Theory

The field emission process is a unique type of electron emission as it is exclusively due to quantum-mechanical effects. Field emission is the emission of electrons from the surface of a solid or liquid into a vacuum due to the presence of high electric fields. In the field emission process, electrons tunnel through the potential barrier at the surface, which the high electric field sufficiently narrows for the electrons to have a non-negligible tunneling probability.

Generally, the Fowler-Nordheim theory [43] is used to quantitatively describe the field emission process for metals. Quantifying the field emission process involves calculating the field emission current density as a function of the electric field. Since this process is essentially a tunneling process, both the tunneling transition probability for the electron to tunnel through the potential barrier and the number of electrons incident on the potential barrier must be found. Integrating these over all energy values gives the desired current density.

Figure 5.1 shows the potential barrier at the surface of a field emitter. Inside the metal, electrons occupy the energy band up to Fermi energy level. The potential energy outside of the metal is regarded as entirely due to the image forces $-e^2/4x$, where x is the distance from the surface of the metal. When an electric field is applied, the field contribution to the potential energy is -eFx, where F is the strength of electric field. Then, the effective barrier can be described by the potential function .

$$U(x) = -\frac{e^2}{4x} - eFx \qquad \text{……..(5.1)}$$

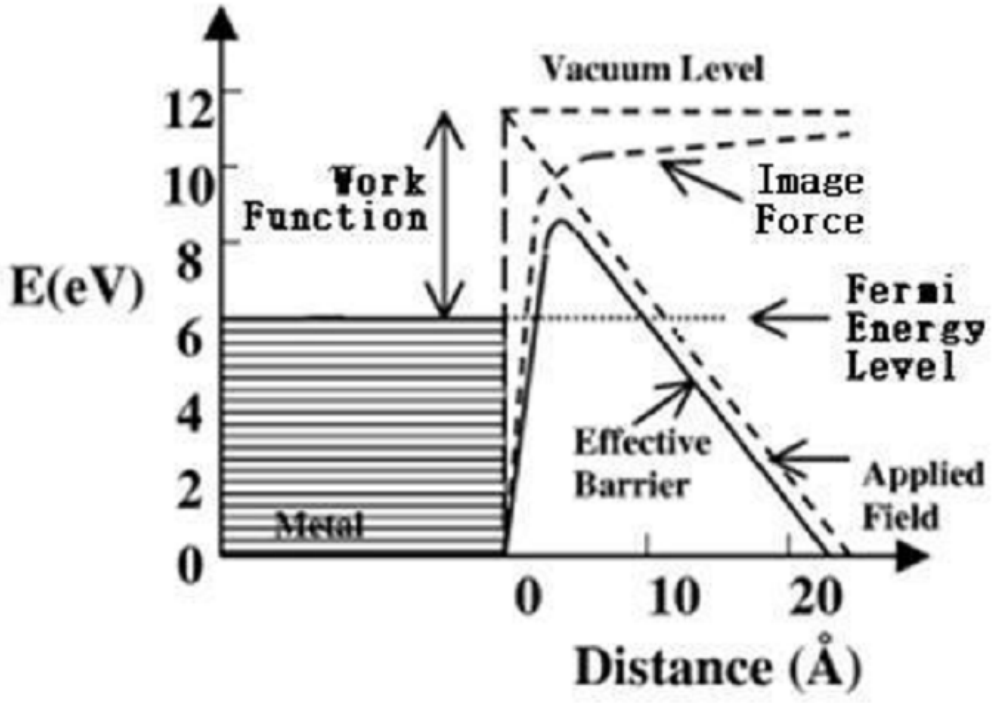

Figure 5.1: Potential Barrier of Field Emitter

The Fowler-Nordheim theory is based on the following main assumptions [34]:

1. The metal obeys the free electron model of Somerfield with Fermi-Dirac Statistics.
2. The metal surface is planar, so the one-dimensional problem is considered. Thus as long as the potential barrier thickness is several orders of magnitude less than the emitter radius, this assumption is justified.

3. The potential within the metal is a constant; the applied electric field does not affect the electron states in the metal.

4. The calculation is performed for the temperature T=0 K.

Under these assumptions, the current density is given by the equation:

$$j = e\int_0^{\infty} n(E_x)D(E_x, F)dE_x \qquad \text{..... (5.2)}$$

where e is the electron charge, $n(E_x)$is the number of electrons per second having energies between E_x and $E_x + dE_x$ incident on 1 cm² of the barrier surface from within the metal, $E_x = p_x/2m$is the part of the electron kinetic energy carried by the momentum component p_x normal to the surface, m is free electron rest mass, D is the barrier transparency and F is the applied electron field.

5.3 Thermal-field Emission

At nonzero temperatures, some electrons occupy energy levels higher than Fermi level. These electrons begin to contribute to the emission current. Emission of this sort is referred to as Thermal-Field emission. In this case, the general Fermi function should be used [34]:

$$f(E_x, T) = \frac{1}{\exp((E_x - E_F)/K_B T) + 1} \quad \text{..... (5.3)}$$

where E_F is the Fermi energy and K_B is the Boltzmann constant.

5.4 Extending the Field Emission Theory

The model of the bulk metal and its surface in Flower-Nordheim theory is highly simplified. With the development of atomically sharp emitters used in tunneling spectroscopy, there came a need to understand the degree of localization of the tunneling process. However, there is no theory that permits accurate calculation of cathode operation characteristics. Some suggested solutions are listed below [34]:

5.4.1 Field Emission from Small-Scale Objects

Many works show that one-dimensional approximation gives a fair description of the field emission process for atomically smooth emitters that have a radius greater than 0.1 m. In this case, the width of the potential barrier is significantly less than the emitters radius of curvature. On the other hand, with field emitters that have a radius of curvature close to or less than the barrier width, the assumptions of one- dimensional barrier and field uniformity over the apex of

the tip are no longer justified. In particular, it is necessary to solve a three-dimensional Schrodinger equation using an asymmetric potential barrier and calculate the behavior of the potential near the surface, accounting for its radius and polar angle variations. As solving such a problem involves formidable difficulties, only rough calculations are made.

5.4.2 Effect of Fermi Surface Structure

The Fowler-Nordheim theory is based on Somerfield's free electron model, and the Flower-Nordheim equation was derived using the Fermi-Dirac energy distribution function. Modern electronic theory of metals is based on the idea that electrons in metals behave as quasi-particles displaying a complex energy dispersion law. Theoretically, the temperature dependence of the field emission differs in principle from what is predicted by the free electron model. In this theory, the emission current decreases instead of increases as in the free electron model.

5.4.3 Many-Particle Effects

Fowler-Nordheim theory is essentially a one-electron theory. There are many phenomena that cannot be described in terms of the one-electron approximation. With the progress made in quantum-field methods due to statistical physics, it became possible to develop a multi-electron theory of field emission. Although there have been many attempts to apply this approach, the calculation of such a problem involves formidable difficulties. At present, the Fowler-Nordheim theory is still the most widely used field emission theory.

5.5 Maximum Field Emission Current Density

One of the most remarkable results of field emission quantum theory is the prediction of very high current density, which is possible due to two factors. (i) if electrons exit the solid by a tunneling mechanism, no energy is required for maintaining the emission process. (ii) There is a very large reservoir of electrons near the Fermi level of a metal. As the density of the electrons in the conduction band is of the order of 10^{22}-$10^{23}cm^{-3}$, the theoretical limit of field emission current density is about $10^{11}A/cm^2$ [34].

5.6 Energy Spectra of Field Emission

The first attempt at measuring an energy distribution of field emitted electrons was made in 1931. Even though the resolution was very poor, this attempt did show that the electrons originated at the Fermi level as Fowler and Nordheim had predicted [21]. The potential distribution near the cathode surface (i.e., the potential barrier at the cathode micro-roughness) is written so:

$$\Phi(x) = \varphi_0 - e/(4x) - \beta U_0 x \qquad \text{…….. (5.4)}$$

where φ_0 is work function, U_0 is cathode surface electric intensity, e is electron charge, x is distance from the cathode, β is the field gain factor. As the potential distribution near the micro-roughness is essentially nonlinear, the equation should be written as

$$\Phi(x) = \varphi_0 - e/(4x) - T(x) \qquad \text{…… (5.5)}$$

Where T(x) is a nonlinear function generally depending on the shape of the micro-roughness. Every shape of the micro-roughness has its own form of the function T(x) . The barrier structure and field emission current density and energy spectrum are significantly determined by the dimensionless parameters $M= \varphi_0/U_0$ a, where is the micro-roughness height [22]. In a number of papers, the possibility of groups of electrons tunneling into a vacuum, correlated in space and time, has been discussed. The first direct measurement of statistical field emission events was reported in 1965. A complete investigation of the statistics of field emission from tungsten shows that its spectra have a single peak. In G. Fursey's experiment, many-particle effects were not observed. This result infers that the multi-peak spectra observed in other's experiments are connected with parasitic secondary emission from intermediate electrodes. In measurements carried out with an intermediate accelerating electrode, a secondary emission multi-peak spectrum was obtained. Later, a detailed investigation of the field emission statistics for different

metals was conducted. The results show with a likelihood of 99.9% accuracy that the field emission from certain metals is a single particle.

5.7 Heating in Field Emission

For many years, it was believed that the major cause of emitter destruction was Joule heating. However, some experiments indicate that the dominant contribution to the thermal balance during field emission is due to Nottingham effect, which is a purely quantum-mechanical energy exchange process. According to this theory, most of the electrons that tunnel through the potential barrier are at lower energy levels than the Fermi level. After these electrons have been emitted into the vacuum, electrons in the conduction band will replace them. As the electrons in the conduction band have higher energy than that of the emitted electrons, they transfer energy to the lattice when replacing the emitted electrons. At a high current density, the energy associated with the Nottingham effect could exceed the energy due to Joule dissipation. Together with Joule heating, Nottingham heating causes a rapid temperature rise in the emitter. After the emitter is heated to a high temperature, most of the emitted electrons are at a higher energy level than the Fermi level; the Nottingham effect begins to cool the cathode. This specific temperature is referred to as the inversion temperature [23]. Joule heating and Nottingham effect together can heat the cathode faster than each of can alone.

The first theoretical analysis of emitter tip self-heating was carried out by W. Dolan et al [36]. They calculated the value of the steady-state maximum current density for a one- dimensional model of an emitter tip. The three-dimensional problem was solved by Glasanov, Baskin, and Fursey using calculations conducted for a tip of the form suggested by Dyke [34]. These calculations took into account Joule heating, Nottingham and Thomson effects, and thermal radiation [24]. The temperature dependence of the resistivity, heat capacity, and surface emissivity were tabulated. The most important result of these calculations is their description of the overheated core's formation inside the emitter apex. The temperature at the surface may be well below the melting point, while in the internal region, it may be equal to several tens of thousands of degrees, leading to enormous temperature gradients and the generation of large thermoelastic stresses. The value of tangential stresses at the tip surface can exceed $2x10^9$ Pa [25], which can destroy the tip before the melting point is reached.

It is known that the maximum attainable field emission current density is limited by Joule Heating of the lattice and Nottingham effect. Whereas Joule Heat is released throughout the bulk of the cathode, the heat produced by Nottingham effect is localized to the near surface region whose thickness is of the order of an electron-phonon free path. Above the Debye temperature, the Nottingham effect is a surface phenomenon. Lowering the emitter temperature causes a significant reduction in Joule heating and a considerable increase in the electron-phonon free path, which shifts Nottingham heating to a bulk effect. Therefore, the maximum field emission current density can be increased by decreasing the emitter temperature [26].

5.8 Field Emission and Vacuum Breakdown

Vacuum breakdown is a complicated phenomenon connected with a large amount of processes in strong electric fields. It is now firmly established that field emission plays an important role in breakdown initiation [27]. In many cases, vacuum breakdown is initiated by the thermal explosion of a micro-tip at the cathode surface, caused by the field emission current. Emitters heated by field emission currents result in thermal instability and transition from field emission to explosive emission and vacuum breakdown [39, 28].

Sometimes breakdown is preceded by the appearance of micro-discharges, low-power pulses of pre-breakdown current, and peak current. The repetition rate of micro-discharges increases with applied voltage. With mass spectrometry, it has been established that micro-discharge currents contain not only an electronic component, but also positive and negative ions [29].

One of the most comprehensive studies in which the DC breakdown mechanism has been confirmed experimentally is that performed by D. Alpert and co-workers [30]. They showed that, taking into account the factor of electron field enhancement at micro-protrusions, local breakdown electric field appears to be independent of gap spacing and is unaffected by electrode geometry. The additional observation that the electric field at which vacuum breakdown takes place is a constant can be interpreted so that breakdown occurs as the density of the field emission current from cathode micro-protrusions reaches a certain value [29, 31].

When a high voltage is applied to a gap for a long time, a variety of processes occur at the electrode and in the gap. It is desirable to identify the processes directly responsible for the initiation of breakdown and domination of the mechanism. In practice, some pre-breakdown processes are either undetectable or they cannot be identified and resolved in space and time.

In numerous experiments, it has been established that breakdown voltage depends to a large extent on electrode material. There is a tendency for the breakdown voltage to increase as the melting temperature and mechanical strength of the electrode material increase. The breakdown voltage is strongly affected by the duration that the voltage is applied and the rate at which voltage is increased. Other factors are also known to influence breakdown voltage, namely, the conditioning of the gap by successive breakdowns, the vacuum conditions, the parameters of the electric circuit in which the gap is connected, the electrode curvature, area and temperature, etc. [28, 29].

5.9 Various Field emission (FE) Structures are

(1) Metal insulator metal

(2) Spindt structure

(3) Carbon nanotubes

(4) Amorphous carbon thin films

5.9.1 Metal-Insulator-metal (MIM)

In a vacuum deposition chamber, nanometer-thick insulating and metal layers are deposited on a metal substrate. The resulting Metal-Insulator-Metal (M-I-M) heterostructure shown in Fig 5.2 can deliver ballistic hot electrons to the surface from the solid side of the vacuum/solid interface. These electrons can induce nonthermal surface chemistry and/or escape into the vacuum. An applied voltage bias between the upper and lower metal layers will cause substrate electrons to tunnel into the conduction band of the insulator, where they ballistically travel across the upper

metal layer to the vacuum interface. The applied bias tunes the energy distribution of the hot electrons to median values ranging from the Fermi level to well above the vacuum level.

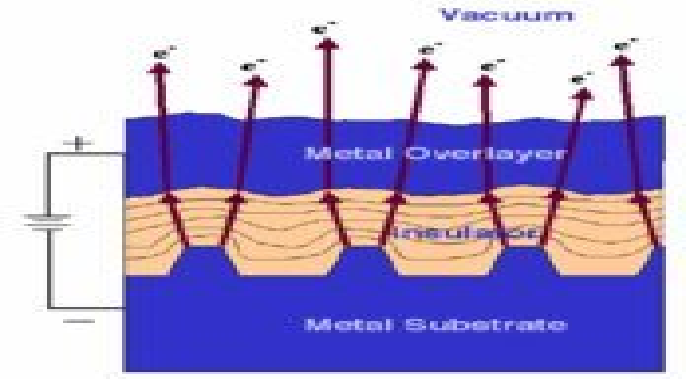

Fig. 5.2 MIM structure.

Performance of MIM is affected by the thickness, roughness, and composition of the metal and insulating layers.

Degradation presents a serious obstacle to practical application of cold emitters based on formed metal-insulator-metal (MIM) structures.

5.9.2 Spindt structures

The low power and light weight of Spindt cathodes (shown in Fig.5.3) makes them ideally suited to space applications requiring electron emission, while the robustness and efficiency of the devices provides the ability to emit currents from nanoamps to tens of milliamps per device tip. Grouped in arrays from a single tip to millions of tips per square centimeter, Spindt cathodes provide a mechanism for emitting controlled current density well above the 1 A/cm^2 level from a low power, cold cathode device limited only by thermal and space charge ejects. Spindt cathodes represent an alternative to traditional electron emission technologies in applications such as space- craft charging measurement and control, gas ionization, plasma contact, electric propulsion, and electron beam emission.

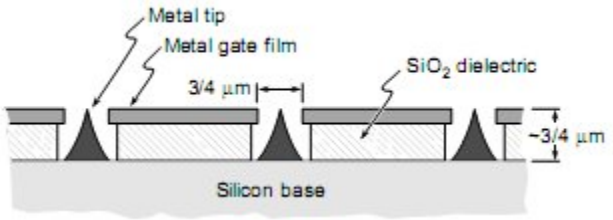

Fig.5.3 Schematic of a Spindt cathode array.

Tip deformation is the measure problem in spindt like structures and they spark at very high voltage. Threshold field is of the order of several hundred V/μm.

5.9.3 Carbon Nanotubes

Field emission displays (FEDs) are making resurgence in the flat panel industry utilizing carbon nanotubes (CNTs) which bypass all of the problems experienced by the preceding FED technology. Carbon nanotubes were first discovered in 1991 by Sumio Ijima in the NEC Research Laboratories of Japan. A carbon nanotube is a very small piece of graphite (a derivative of carbon) rolled up into a very small tube. It is not a metal but a very strong structure built entirely out of covalent bonds with field emitting properties. Made by reducing a sheet of graphite so that it becomes a narrow strip approaching 30 nm, the strip curls up and forms a tube with a diameter of 10 nm – this singular tube is known as a single-walled nanotube (SWNT). Multiple walled nanotubes (MWNT) are several SWNTs (Fig. 5.4) nested inside one another where each carbon atom is bound to three other carbon atoms. The exact arrangement of carbon atoms, and whether the tubes are open-ended or closed, can determine whether these CNTs are semiconducting or conducting. CNTs are chemically stable therefore they only react under extreme conditions such as extremely high temperatures (2500^0C) with oxygen or hydrogen; consequently, the problems of reacting with resident gases, overheating, or tip deformation are solved with CNTs.

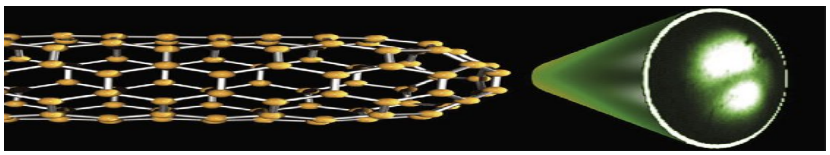

Fig.5.4 Single wall carbon nano tube (SWNT)

Major drawback in CNT is that it is used in powder form so degassing is a big problem in high vacuum. For this filtration of CNTs and separation from the powder is a tedious task.

CNTs field emission occurs at very low threshold voltage (1-3V/μm) and the current density is high (few mA/cm^2) but the current sustain for small period of time hence it is very hard to make display. Amorphous carbon gives the alternative for display because it is used in thin film.

Other drawback with CNTs is that they are mostly multiwalled not singlewalled which is not suitable for field emission display.

5.9.4 Amorphous carbon film

Why Amorphous Carbon thin film for Field emission (FE)

Electron field emission (EFE) from amorphous carbon (a-C) films [44, 45] has been widely investigated due to its outstanding emission properties such as

(a) Low microscopic emission field [46, 47].

(b) Unique chemical, electrical, optical, and mechanical properties.

(c) Low Electron affinity.

(d) Space charge induced band bending.

(e) Easy to grow amorphous structure.

5.10 Mechanism of field emission in a-C film

a-C film is formed from carbon atoms with mainly sp^2 and sp^3 bonding. Electronic properties of a-C films strongly depend on the sp^2 content of the film as well as the presence, size distribution of sp2 bonded clusters within the sp^3 matrix. For instance, electrical conductivity of a-C films are governed through the hopping of electrons between the conductive sp^2 clusters and hence depends on the microstructure and orientation of sp^2 bonded atoms [48,49] as shown in Fig. 5.5 .These unique sp^2 clusters will also provide a local enhancement mechanism which results in electron emission at very low macroscopic fields.

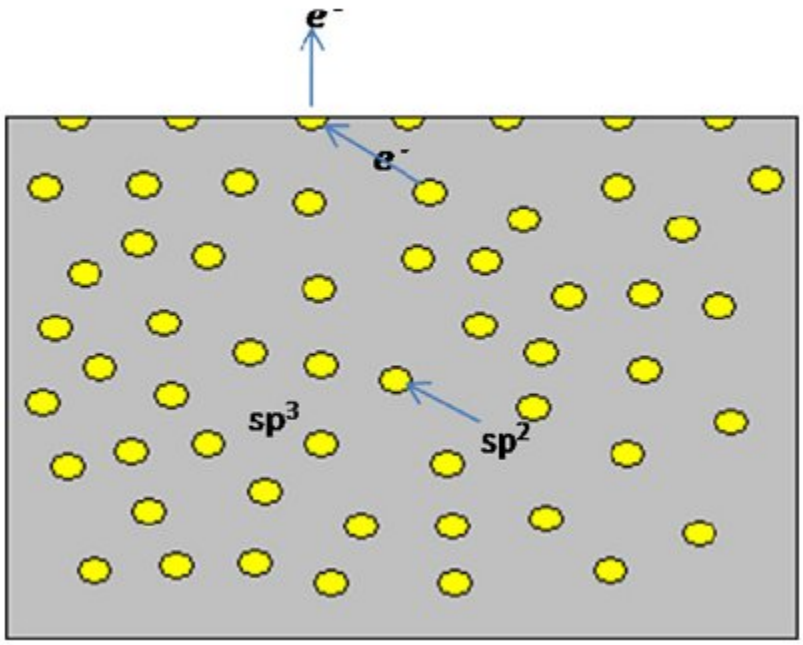

Fig 5.5 Schematic representation of FE from carbon film .The film is formed from sp^2 nanoclusters (yellow spheres) embedded in insulating sp^3 bonded matrix.

5.11 Field Emission Device (FED)

A field emission display (FED) is a flat panel display technology that uses large-area field electron sources to provide electrons that strike colored phosphor to produce a color image. In a general sense, a FED consists of a matrix of cathode ray tubes, each tube producing a single sub-pixel, grouped in threes to form red-green-blue (RGB) pixels.

Field emission displays, electrons coming from millions of tiny microtips pass through gates and light up pixels on a screen. This principle is similar to that of cathode-ray tubes in television sets. The difference: Instead of just one "gun" spraying electrons against the inside of the screens face, there are as many as 500 million of them (microtips) as shown in Fig.5.6. Comparisons of different displays available in the market are summarized in table 5.1.

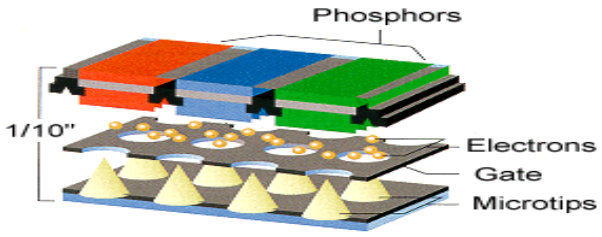

Fig.5.6. Schematic diagram of FE Device.

Table 5.1 Comparison of different technology with FE display.

Technology	Luminous Efficiency (Lm/W)
Cathode Ray Tube (CRT) (at 30KV)	3
Plasma Display Panel (PDP)	0.8
Liquid Crystal Display (LCD)	3
Organic Light Emitting Diode (OLED) / Polymer light-emitting diodes (PLED)	5
Field Emission Display (FED) at 8 KV	7

5.11.1 Advantage of Field Emission Display (FED)

(a)Inherently high luminous efficiency

(b)No Response Time issues

(c)CRT-like Color Gamut

(d)Lower Power Consumption

(i) Cold Cathode Emission

(ii) Distance between cathode and screen ~0.2–5mm

(e)Flat Panel Technology

(i)Matrix Addressed – No Delay.

5.11.2 FED Technology Roadblocks

(a)High cost of submicron technology

(b)High Voltage Breakdown due to electron bombardment and spacer charging

(c)Phosphor decay in case anode is at low voltage to counter the above problem

(d)Backscatter from anodes at high anode voltages leading to cross talk

5.12 Experimental setup and results

5.12.1 Experimental set up consists of the following:

(i) a-C film grown on silicon substrate given a negative bias.

(ii) An Indium tin oxide coated glass positive bias

(iii) A spacer of thickness 50-150 micron placed between them to protect the short circuit.

This whole system is placed in a high vacuum (of the order of 10^{-7} Torr) as shown in Fig.5.7. Simulation of threshold voltage and emitted current is done with the help of computer which is interfaced with the device. Field emitted current is measured step by step increasing the high voltage bias using high voltage source meter whose maximum rating is 1100 V and 1A current. $E_{turn\ on}$ and emitted current density (J) [J is defined by dividing emitted current (I) to the area of the hole in the spacer is noted down]. $E_{turn\ on\ is}$ evaluated corresponding to 1μA current measured in the device.

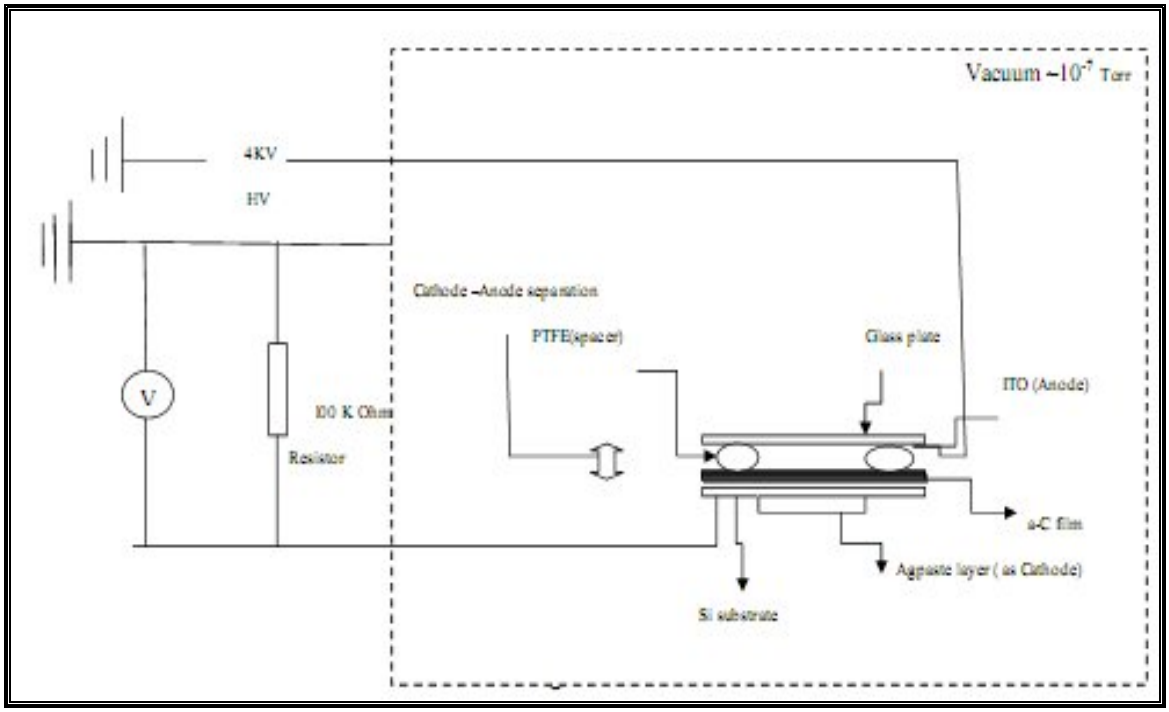

Fig. 5.7 Schematic of the experimental setup used to study the field emission from a-C thin film having embedded nanoparticles.

5.12.2 Field emitted current density (J) vs applied electric field (E)

Field emitted current density (J) verses applied electric field of the a-C films having embedded nanoparticles as shown in fig.5.8.

Electric field is evaluated by taking the ratio of voltage applied to the thickness of the PTFE spacer.

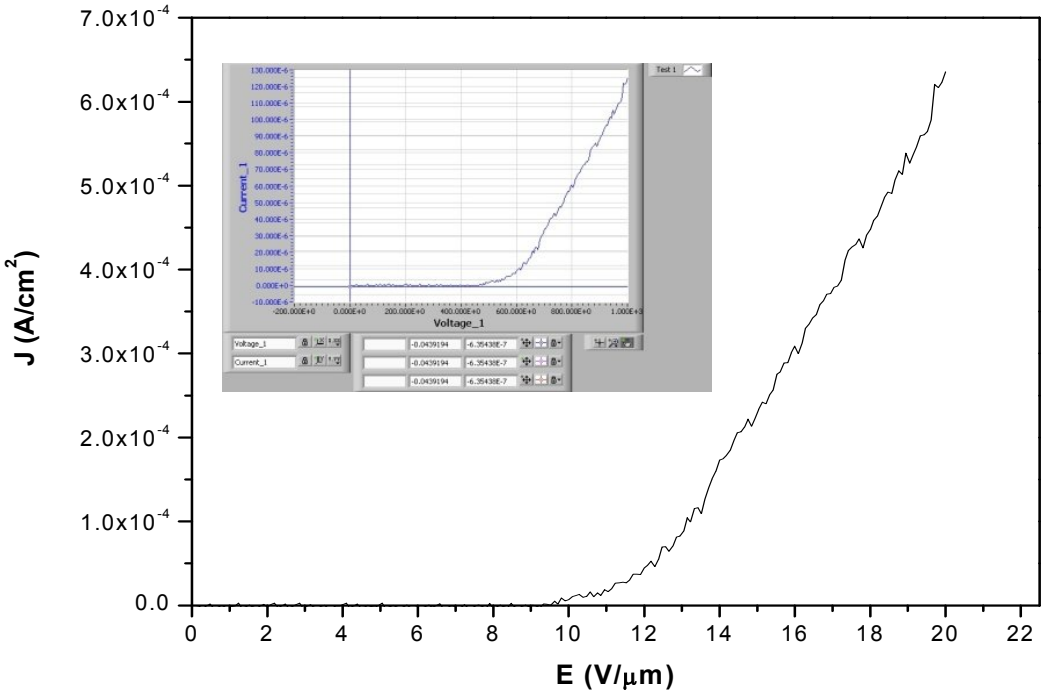

Fig 5.8 Shows the Field emitted current density versus the applied electric field in the field emission experiment of a-C films.

$E_{turn\ on}$ was found to be 9.1(V/μm) and current density (J) at 1050 V (21V/μm) was found to be 6.6 $x10^{-4}$ (A/cm^2) in a-C film. Current density is ~1mA/cm^2 range hence it can be used in making Field emission Device.

5.12.3 Field Emission Device (FED)

We attempted to make the Field emission display (FED) device. The schematic of the FED device is shown in the Fig. 5.9.

This device consists of the following:

(i) Cathode-amorphous carbon thin films grown by CJCA on Silicon substrate.

(ii) Anode-An ITO (Indium Titanium Oxide).

(iii) ZnO phosphor on ITO coated glass substrate.

(iv) A PTFE Spacer of 150 micrometer thickness was used in between the cathode and anode.

(v) High vacuum is of the order of 10^{-7} Torr.

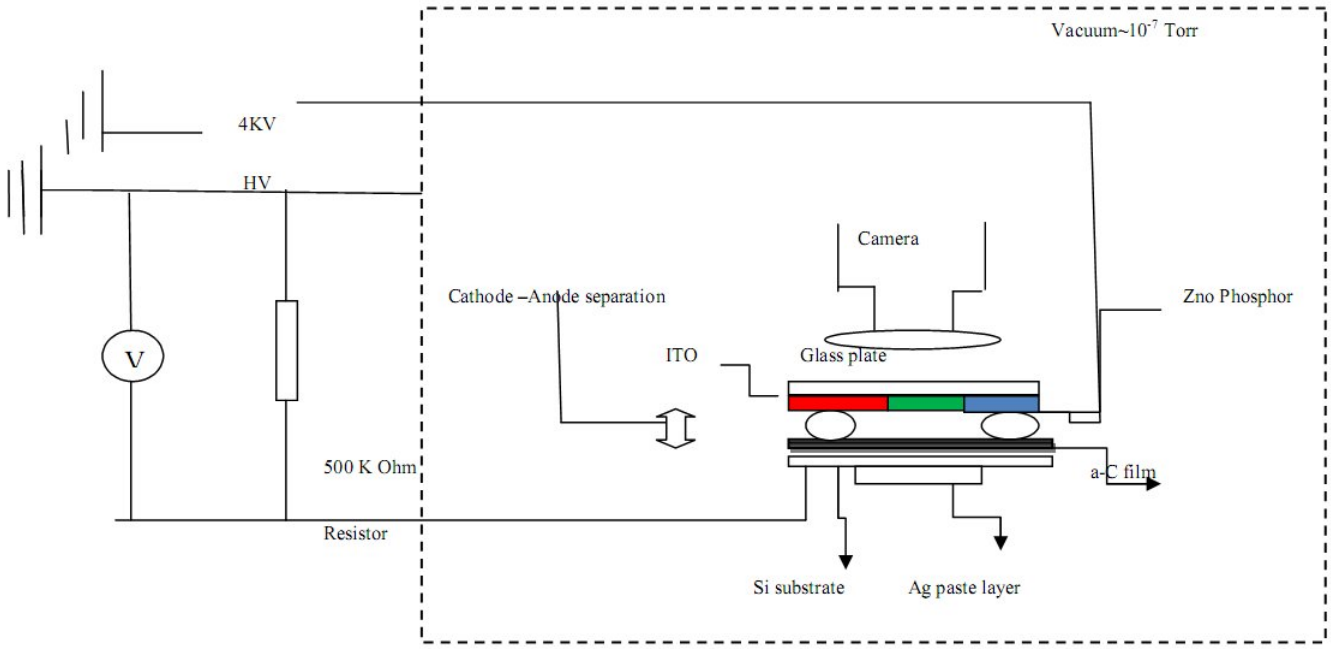

Fig. 5.9 Schematic of Field emission display device design.

5.12.4 Phosphor coating

Phosphor coating on ITO coated glass substrate was attempted by thermal evaporation method as shown in Fig 5.10.

- Zinc powder is taken in the quartz boat. Heated in presence of oxygen gas at a temperature of 800^0 C for about 2 hours.
- ITO coated glass samples are placed at some distance from the center of furnace.
- Coating of ZnO is disposed on the ITO coated glass.

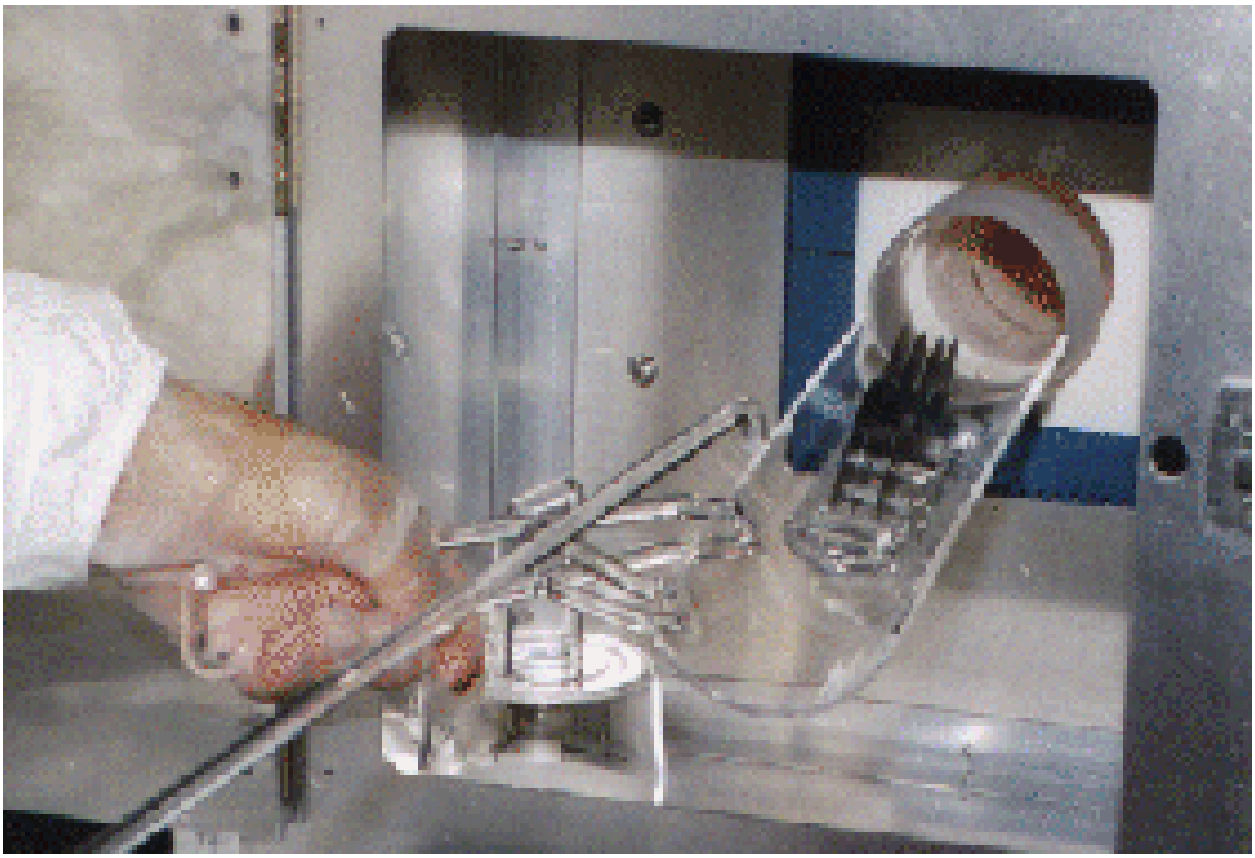

Fig. 5.10 Experimental Process for phosphor coating

In Photoluminescence it was found that the ZnO phosphor did not adhere well with the ITO coated glass substrate.

So we tried sticking phosphor on ITO coated glass by some adhesive but it was also degassing inside the vacuum chamber when we tried to measure the field emitted current. There was a rise of pressure by two orders so we could not carry out the field emission measurement and could not finally observe the display.

CHAPTER 6

CONCLUSION

In this study, amorphous carbon thin films having embedded nanoparticles have been deposited by a novel cathodic jet carbon arc technique. X-Ray diffraction data indicates the amorphous nature of the film having nano particles. SEM images exhibits the presence of nanoparticles in film. AFM micrograph shows that the film deposited is having smooth surface. Electrical conductivity measurement carried out at varying temperature indicates that there is a thermally activated process. The conductivity of the film is very high in order~ 10 $ohm^{-1}cm^{-1}$ in comparison to the value reported in literature. The cause of high conductivity may be related to the presence of nano particles.

Finally amorphous carbon thin film having embedded nanoparticles was used as emitters in field emission display process. The threshold field of emission corresponding to 1μA current was observed as 9.1 V/μm and maximum emission current density of 0.66 mA/cm^2 was observed at 21V/μm electric field. The emission current density observed in a-C film having embedded nanoparticles is approaching the value obtained in carbon nanotubes (~ $1mA/cm^2$).

We tried to make the display device but degassing of phosphor was the hurdle which was not overcome but it is the future work. The remainder of this chapter includes the conclusion of the main experimental results.

REFERENCES

(1)D. Fujita, “Fabrication of Carbon Nanowires without External Carbon Source”, National Institute Materials Science, Volume Number 3, September 2003.

(2)J. Boyd, “Samsung's Plasma Displays Barred from Japanese Market”, IEEE Spectrum, Volume 41.

(3)Z Ying, Q Wan, Z T Song and S L Feng, “SnO2 Nanowhiskers and their Ethanol Sensing Characteristics”, Nanotechnology Volume 15.

(4) H. Busta, “Vacuum Microelectronics-1992”, Journal of Micromechanics Microengineering, Volume 2.

(5) G. Yuan, H. Song, Y. Jin, H. Mimura and K. Yokoo, “Effect of Distribution of Field Enhancement Factor on Field Emission from Cathode with A Large Number of Emission Sites”,Thin Solid Films, Volume 484.

(6)Y. Khlifi, K. Kassmi, L. Roubi and R. Maimouni, “Modeling of Fowlor- Nordheim Current of Metal/ultra-thin Oxide/semiconductor Structures”, M. J. Condensed Matter, Volume 3, Number 1.

(7)J. Boyd, “Samsung's Plasma Displays Barred from Japanese Market”, IEEE Spectrum, Volume 41.

(8)Vitalis and synthesis of urea. From Friedrich Wohler to Hans A. Krebs by Kinne-Saffran E, Kinne RK. Max-Planck-Institut fur molekulare Physiologie, Dortmund, Germany. UAm J Nephro*l*. 1999.

(9) Ekimov, et al. (2004) Nature 428:542–545].

(10) D. R. McKenzie, Rep. Prog. Mater. 5, 388 (1996).

(11) Edison, T.A., Manuscript patent application, in Edison papers project, unpublished. 1884.

(12) M.D. Blue and G.C. Danielson Journal of applied physics 28.583(1957).

(13) Lucas etal. Rev.Sci Inst 32 (1960).

(14) M. Kikuchi, S.N., H. Ohmura, S. Oketani, Structures of metal films produced by vacuum-arc evaporation method. J. Appl. Phys., 1965. **4**: p. 940.

(15) Sablev et al. U.S. Patent No.-3783231.

(16) Snaper et al. U.S. Patent No.-3625848.

(17) Brandolf. Vapor deposition apparatus and method. Patent No.-: 4511593

(18) Soviet journal of Plasma Physics 1978.

(19) B.K Tay, Material science and engenring R 52 (2006)1-48 Review of metal oxide film deposited by filtered cathodic vacuum arc deposition technique.

(20) G. G. Stoney, Proc. R. Soc. London, **A82**, 553, p 172 (1909).

(21) Gadzuk, J.W.1., and Plummer, E.W.1., "Field emission energy distribution (FEED)," Reviews of Modern Physics, Vol. 45, No. 3, 1973, pp. 487-548.

(22) Rodnevich, B.B., "Energy spectrum of field emission," Vacuum Microelectronics Conference, *1996*. IVMC'96., 9th International, 1996, pp. 77-80.

(23) Charbonnier, F.M., Strayer, R.W., Swanson, L.W., "Nottingham Effect in Field and $T- F$ Emission: Heating and Cooling Domains, and Inversion Temperature," Physical Review Letters, Vol. 13, No. 13, 1964, pp. 397-401.

(24) Glazanov, D.V., Baskin, L.M., and Fursei, G.N., "Kinetics of the pulsed heating of field-emission cathode points with real geometry by a high-density emission current," Soviet Physics - Technical Physics, Vol. 34, No. 5, 1989, pp. 534-9.

(25) Baskin, L.M., Glazanov, D.V., and Fursei, G.N., "Influence of thermoelastic stresses on the destruction of field-emission cathode points and the transition to explosive emission," *Soviet* Physics - Technical Physics, Vol. 34, No. 5, 1989, pp. 579-80.

(26) Bugaev, S.P., Litvinov, E.A., Mesyats, G.A., "Explosive emission of electrons," Uspekhi Fizicheskii Nauk, Vol. 115, No. 1, 1975, pp. 101-20.

(27) Su, Y., Chen, W., Wang, F., "Cathode spots on the surface of nanostructured W alloys," Materials Letters, Vol. 59, No. 8-9, 2005, pp. 1046-1049.

(28) Mesyats, G.A., "Explosive Electron Emission," URO-Press, Ekaterinburg, 1998, pp. 248.

(29) Mesyats, G.A., "Cathode Phenomena in a Vacuum Discharge: The Breakdown, the Spark and the Arc," Nauka Publishers, MOSCOW, 2000,

(30) Alpert, D., Lee, D.A., Lyman, E.M., "Initiation of Electrical Breakdown in Ultrahigh Vacuum," Journal of Vacuum Science and Technology, Vol. 1, No. 2, 1964, pp. 35-50.

(31) Chatterton, P.A., "A theoretical study of field emission initiated vacuum breakdown," Proceedings of the Physical Society, Vol. 88, No. 1, 1966, pp. 231-245.

(32) Wood, R.W., "A New Form of Cathode Discharge and the Production of X-Rays, together with Some Notes on Diffraction. Preliminary Communication," Phys.Rev.(Series I), Vol. 5, No. 1, 1897, pp. 1-10.

(33) Fowler, R.H., and Nordheim, L., "Electron Emission in Intense Electric Fields," Proceedings of the Royal Society of London.Series A, Containing Papers of a Mathematical and Physical Character, Vol. 119, No. 781, 1928, pp. 173-181.

(34) Fursey, G., "Field emission in vacuum microelectronics," Microdevices, Kluwer Academic/Plenum Publishers, New York, 2005, pp. xv, 205 p.

(35) Henderson, J.E., and Dahlstrom, R.K., "The Energy Distribution in Field Emission," Phys.Rev., Vol. 55, No. 5, 1939, pp. 473-481.

(36) Dolan, W.W., Dyke, W.P., and Trolan, J.K., "The Field Emission Initiated Vacuum Arc. II. The Resistively Heated Emitter," Phys.Re*v.,* Vol. 91, No. 5, 1953, pp. 1054- 1057.

(37) Dyke, W.P., and Trolan, J.K., "Field Emission: Large Current Densities, Space Charge, and the Vacuum Arc," Phys.Rev.*,* Vol. 89, No. 4, 1953, pp. 799-808.

(38) Charbonnier, F.M., Barbour, J.P., Brewster, J.L., "Intense, Nanosecond Electron Beams," Proceedings of the 2nd IEEE Particle Accelerator Conference, Vol. NS-14, 1967, pp. 789.

(39) Fursey, G.N., "Field Emission and Vacuum Breakdown," Electrical Insulation, IEEE Transactions on [See also Dielectrics and Electrical Insulation, IEEE Transactions on], Vol. EI-20, No. 4, 1985, pp. 659-670.

(40) Crewe, A.V., Eggenberger, D.N., Wall, J., "Electron Gun Using a Field Emission Source," Review of Scientific Instruments*,* Vol. 39, No. 4, 1968, pp. 576-583.

(41) Spindt, C.A., Holland, C.E., Brodie, I., "Field-emitter arrays to vacuum fluorescent display," Electron Devices, IEEE Transactions on*,* Vol. 36, No. 1; essentially a miniature cathode-ray tube (CRT), the device has the potential to produce brightness similar to those on a CRT in a panel that is 3.3 in square (8.4 cm) in area and 0.15 in (4 mm) thick, 1989, pp. 225-228.

(42) Bell, A.E., and Swanson, L.W., "Total energy distributions of field-emitted electrons at high current density," Physical Review B (Condensed Matter)*,* Vol. 19, No. 7, 1979, pp. 3353-64.

(43) Fowler, R.H., and Nordheim, L., "Electron Emission in Intense Electric Fields," Proceedings of the Royal Society of London.Series A*,* Containing Papers of a Mathematical and Physical Character*,* Vol. 119, No. 781, 1928, pp. 173-181.

(44) Robertson J. Diamond-l ike amorphous carbon. Mater Sci Eng R 2002;37(4–6):129 –281.

(45) Cheah LK, Shi X, Liu E, Tay BK. Electron field emissi on properties of tetrahedral amorphous carbon films. J Appl Phys 1999;85(9):6816–21.

(46) Satyanarayana BS, Hart A, Milne WI, Robertson J. Field emission from tetrahedral amorphous carbon. Appl Phys Lett 1997;71(10):143 0–2.

(47) Feng Z, Brown IG, A g e r III JW. Electron emissio n from chemical vapor deposited diamond and amorphous carbon films observed with a simple field emissio n d evice. J Mater Res 1995;10(7):1585 –8. 2

(48) Carey J D, Silva SRP. Disorder, clusteri ng, and locali zation effects in amorphous carbon. Phys Rev B 2004;70(23):1–8

(49) O.S.Panwar*,SushilKumar, S.S.Rajput, RajnishSharma ,R.Bhattacharyya ‘Dependence of field-emission threshold in diamond-like carbon films grown by various techniques’ Vacuum72(2004)183–192.